JHEP

Published for SISSA by Springer

Received: December 8, 2016
Revised: January 30, 2017
Accepted: January 31, 2017
Published: February 7, 2017

Stellar cooling bounds on new light particles: plasma mixing effects

Edward Hardy[a] **and Robert Lasenby**[b]

[a] *Abdus Salam International Centre for Theoretical Physics, Strada Costiera 11, 34151, Trieste, Italy*
[b] *Perimeter Institute for Theoretical Physics, 31 Caroline Street N, Waterloo, Ontario N2L 2Y5, Canada*

E-mail: ehardy@ictp.it, rlasenby@perimeterinstitute.ca

Abstract: Strong constraints on the coupling of new light particles to the Standard Model (SM) arise from their production in the hot cores of stars, and the effects of this on stellar cooling. For new light particles which have an effective in-medium mixing with the photon, plasma effects can result in parametrically different production rates to those obtained from a naive calculation. Taking these previously-neglected contributions into account, we make updated estimates for the stellar cooling bounds on light scalars and vectors with a variety of SM couplings. In particular, we improve the bounds on light ($m \lesssim$ keV) scalars coupling to electrons or nucleons by up to 3 orders of magnitude in the coupling squared, significantly revise the supernova cooling bounds on dark photon couplings, and qualitatively change the mass dependence of stellar bounds on new vectors. Scalars with mass $\lesssim 2\,\mathrm{keV}$ that couple through the Higgs portal are constrained to mixing angle $\sin\theta \lesssim 3 \times 10^{-10}$, which gives the dominant bound for scalar masses above $\sim 0.2\mathrm{eV}$.

Keywords: Beyond Standard Model, Thermal Field Theory

ArXiv ePrint: 1611.05852

doi:10.1007/JHEP02(2017)033

JHEP02(2017)033

Contents

JHEP02(2017)033

1 Introduction

Many Beyond-Standard-Model (BSM) physics scenarios include new light, weakly-coupled particles. If a new particle has mass $\lesssim 100\,\mathrm{MeV}$, then it will be produced in the hot cores of stars/supernovae, and will contribute to energy transport in the star. The non-observation of anomalous energy transport, in various different types of star, can then place strong constraints on the coupling of the particle to the Standard Model (SM) particles that make up the star [1]. These bounds are often referred to as 'stellar cooling', though they more properly correspond to anomalous energy loss or transport.

Previous calculations of particle production in stars have often assumed that a simple 'kinetic theory' calculation, using in-vacuum matrix elements for processes producing the new state, with thermal abundances for the SM initial and final states, is a good approximation ([2–5] are some examples). However, the large electron density in stellar cores results in large characteristic plasma frequencies, giving non-negligible collective effects. These are especially important for new light particles that gain an in-medium mixing with SM excitations. In particular, if the new particle is light compared to the thermal mass of the SM excitation, then such mixing effects can parametrically change the production rate, compared to the naive kinetic theory estimate.

These phenomena have been taken into account for dark photon emission from stars (not including supernovae) in [6, 7], after their possible importance was first identified by [8]. In this work, we point about that similar effects hold for other forms of BSM particle interactions, and can lead to important changes in stellar cooling constraints. In the case of dark photon, these effects can be included by choosing a sterile/active basis, in which the sterile mode couples to the medium purely through its Lagrangian mass mixing. However, such a basis choice is not generically possible, and we explain how to compute production rates in more general cases. We also extend the analysis of dark photon production to include energy loss from core-collapse supernovae, correcting previous literature which used the kinetic theory approximation [4, 5, 9], and to take into account trapping constraints in stars. The resulting constraints are shown in figure 3.

New light vectors which couple coherently to SM plasma oscillations have an in-medium mixing with the SM photon. At vector masses well below the stellar plasma frequency, this mixing suppresses the production rate. At masses around the plasma frequency, resonant conversion of SM photons to the new vector can enhance the production rate, while at masses above the plasma frequency the kinetic theory approximation holds. Figure 4 shows how this changes the solar bounds on a massive $B - L$ vector.

New light scalars can mix with SM plasmons — the in-medium 'longitudinal mode of the photon' [1]. Since the plasmon dispersion relation crosses the light-cone, resonant production of the light scalar is possible down to arbitrarily low scalar masses, and unlike the case for a light vector, is not suppressed by powers of the mass. So, for scalar masses below the stellar plasma frequency, resonant production can dominate, parametrically strengthening the stellar cooling bounds. Figure 6 shows this effect for a light Higgs-portal scalar. Quantitatively, we improve previous coupling bounds by a factor of $\sim 10^3$ (in the coupling squared) for both a $\phi\bar{e}e$ coupling, and a scalar coupling to nucleons.

JHEP02(2017)033

While light scalar or vectors are the simplest cases, mixing effects may also be important for other new particle candidates, the detailed investigation of which we leave to future work. For some candidates, symmetries of the low-energy theory prevent an in-medium mixing with SM states (e.g. charge conservation for a milli-charged particle, or parity for an axion-like particle). However, plasma effects may still have an important impact on thermal production rates of such particles (via screening, thermal masses, etc.), although we will not discuss them here. In addition to stellar cooling, there are also other physical scenarios in which our calculations may be useful, among them early-universe cosmology.

The main aim of this paper is to illustrate how plasma mixing effects may have important consequences for the thermal production of new light particles, not to calculate precise and robust constraints on such particles. Consequently, we do not do the detailed stellar modelling that would be required to derive properly reliable bounds, instead taking representative stellar models and approximate analytic versions of observational bounds from the literature. However, this suffices to demonstrate the parametric changes that our new physical effects bring about, and shows that they would have important effects in a detailed analysis.

The structure of this paper is as follows: in section 2 we introduce the machinery of thermal field theory, and obtain the proper expressions for production rates of new light BSM states. Following this, in section 3 we apply these results to stellar cooling, and update the constraints on BSM couplings from observations. Finally, in section 4, we discuss our results, and review directions for future work.

2 Thermal production rates and plasma mixing

The conceptually-simplest way to handle medium effects in a thermalised plasma, such as that found in a stellar core, is to use the apparatus of thermal field theory (TFT) — for a comprehensive overview, see e.g. [10]. In this framework, weakly-coupled excitations in a medium correspond to poles in the thermal propagators of fields, with the decay and production rates of these excitations being related to the imaginary parts of the pole locations. If we have a state X that couples weakly to the species making up a thermalised bath, then writing the thermal propagator in terms of the free propagator and the 'thermal self-energy', $D_X = \frac{1}{D_X^F - \Pi_X}$, we are interested in the imaginary part of Π_X (see appendix A for a short review of propagators in the real-time thermal field theory formalism).

This paper's central point is that, if X mixes with the bath fields, either through terms in the Lagrangian, or through medium-induced effects, then Π_X is not just given by the sum of one-particle-irreducible (1PI) TFT diagrams. Instead, diagrams with intermediate bath species propagators must also be included. This is illustrated, in the case where X mixes with a single bath species A, by figure 1. At the level of a leading-order 'kinetic theory' calculation, the extra terms correspond to including X production through its medium-induced mixing with A. This point may seem trivial, but we will see that many calculations in the literature correspond to ignoring mixing effects, which can lead to parametrically incorrect results.

JHEP02(2017)033

To see the effects of mixing more explicitly, we can consider the species-non-diagonal terms. Supposing again that X mixes with a single bath species A (in the models we consider, A will generally be the SM photon), the in-medium propagation eigenstates will be given by null eigenvectors of the 2×2 matrix

$$\begin{pmatrix} K^2 - \Pi^{AA} & -\Pi^{AX} \\ -\Pi^{XA} & K^2 - m_X^2 - \Pi^{XX} \end{pmatrix} , \tag{2.1}$$

where $K = (\omega, \vec{k})$ is the 4-momentum, and we have taken $m_A = 0$. Here, the self-energies Π^{AX} etc. *do* correspond to the sum of 1PI diagrams (evaluated at real energy-momentum). If the couplings of X to bath states are $\mathcal{O}(g)$, where g is small, then since $\Pi^{AX} = \mathcal{O}(g)$ and $\Pi^{XX} = \mathcal{O}(g^2)$, for a given $\vec{k}$ there exist null eigenvectors when

$$\omega_c^2 = k^2 + \Pi^{AA} + \frac{(\Pi^{AX})^2}{\Pi^{AA} - m^2} + \mathcal{O}(g^4) , \tag{2.2}$$

$$\omega_c^2 = k^2 + m^2 + \left(\Pi^{XX} - \frac{(\Pi^{AX})^2}{\Pi^{AA} - m^2} \right) + \mathcal{O}(g^4) , \tag{2.3}$$

where $\omega_c \equiv \omega + i\omega_i$ is the complex frequency. The second expression corresponds to the weakly-coupled state, and we can see how the self-energy corresponds to the sum of the terms from figure 1. These expressions make sense if g is small compared to all other parameters. In particular, if $\Pi^{AA} - m^2$ becomes very small ('on-resonance'), they may cease to apply, as discussed in section 2.2. The canonically-normalised propagation eigenstates are, in the (A, X) basis,

$$\sqrt{Z_A^{-1}} \begin{pmatrix} 1 \\ \frac{\Pi^{AX}}{\Pi^{AA} - m^2} \end{pmatrix} + \mathcal{O}(g^2) \quad , \quad \begin{pmatrix} -\frac{\Pi^{AX}}{\Pi^{AA} - m^2} \\ 1 \end{pmatrix} + \mathcal{O}(g^2) , \tag{2.4}$$

where

$$Z_A^{-1} \equiv 1 - \frac{d\,\mathrm{Re}\Pi}{d\omega^2} , \tag{2.5}$$

is the wavefunction renormalisation factor for A, with the derivative being evaluated on-mass-shell. The renormalisation factor for the mostly-X eigenstate is $1 + \mathcal{O}(g^2)$.

The mostly-X eigenstate has at least g-suppressed interactions with the thermal bath. So, if the bath is of finite size (such as a star) and g is small enough, it will free-stream out of the bath, rather than coming to thermal equilibrium. In this case, we are interested in the production rate of X by the bath. If the order-g couplings of X to the bath involve production/absorption of one X, rather than scattering of X, then the production rate can be related, via detailed balance, to the damping rate given by the imaginary part of the frequency. Since the production and absorption rates satisfy $\Gamma_{\mathrm{prod}} = e^{-\omega/T}\Gamma_{\mathrm{abs}}$, and the overall damping rate is $\Gamma = \Gamma_{\mathrm{abs}} - \Gamma_{\mathrm{prod}}$ (for a bosonic excitation), we have $\Gamma_{\mathrm{prod}} = f_B(\omega)\Gamma$, where $f_B(E) \equiv (e^{E/T} - 1)^{-1}$ is the bosonic thermal occupation number. The production rate per volume for the (assumed bosonic) mostly-X state is therefore given by

$$\frac{dN_{\mathrm{prod}}}{dV\,dt} = \int \frac{d^3k}{(2\pi)^3} \Gamma_{\mathrm{prod}} = -\int \frac{d^3k}{(2\pi)^3} \frac{f_B(\omega)}{\omega} \,\mathrm{Im} \left(\Pi^{XX} - \frac{(\Pi^{AX})^2}{\Pi^{AA} - m^2} \right) + \mathcal{O}(g^4) . \tag{2.6}$$

JHEP02(2017)033

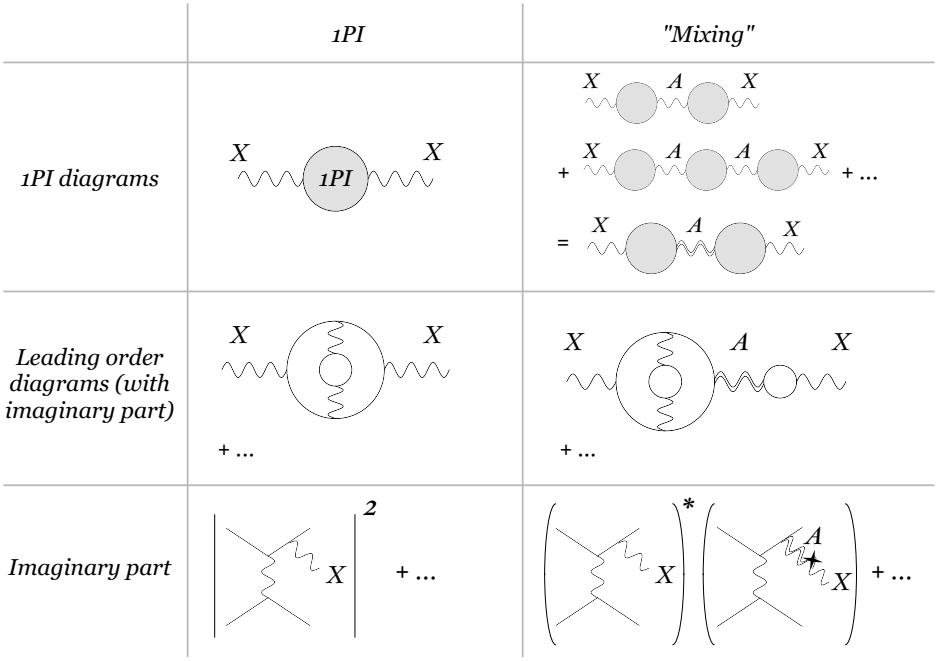

Figure 1. Illustration of the 1PI contributions to the thermal field theory self-energy of a particle X, versus the 'mixing' contributions involving intermediate bath species propagators, where we take X to mix with a single bath species A. The double-lined A propagator indicates the full (resummed) TFT propagator. The third row shows some of the tree-level contributions to the imaginary part of the self-energy, with the 'mixing' diagrams corresponding to X production involving its medium-induced mixing with A (indicated by the star). Many calculations of thermal particle production in the literature only consider the class of diagrams show in the 1PI column, ignoring the 'mixing' contributions.

The essential point of this paper is that, for production of new weakly-interacting particles from a SM bath, many previous analyses correspond to only considering the Π^{XX} term, whereas in fact the other term can sometimes be very important.[1] One straightforward example where this cannot be ignored is the case of low-mass dark photon production, as has been noted in a number of papers [6–8]. We will see that this also occurs in other cases of phenomenological interest.

2.1 SM plasma oscillations

Suppose that there exists an as-yet-undiscovered light bosonic state, which couples weakly to the SM (a new fermionic state, if it is not detectably SM-charged, can only mix with the SM neutrinos, and such a mixing would not be important in most scenarios we consider). If this state does not carry SM quantum numbers, then, in the TFT treatment of a low-energy ($T \ll \Lambda_{\rm QCD}$) SM plasma, it can only mix with the photon field. In this section,

[1] An additional point is that, though we have calculated these 'mixing effects' within the thermal field theory framework, they are better thought of as 'plasma' effects rather than 'thermal ones', and will also occur out of thermal equilibrium. Appendix G works out a particular case by considering classical plasma oscillations in the fluid approximation, with the presence of a new weakly-coupled field in addition to electromagnetism; this gives a toy example of a non-thermal calculation of this kind.

JHEP02(2017)033

we review the photon field's TFT behaviour (more comprehensive reviews can be found in [1, 11]).

We can write the in-medium photon self-energy, in an isotropic medium, as

$$\Pi_{\mu\nu}(K) = (\epsilon^+_\mu \epsilon^{+*}_\nu + \epsilon^-_\mu \epsilon^{-*}_\nu)\Pi_T + \epsilon^L_\mu \epsilon^L_\nu \Pi_L \,, \tag{2.7}$$

where $\epsilon^\pm$ are the usual orthogonal polarisation vectors [1], and $\epsilon^L_\mu = \frac{1}{\sqrt{K^2}}(-|k|, \omega\hat{\vec{k}})$ is the longitudinal polarisation vector (working in the rest frame of the medium). We will write $\Pi = \Pi_r + i\Pi_i$ for the real and imaginary parts of the self-energy. For a non-relativistic, dilute plasma, the real parts are [1]

$$\Pi_{T,r} = \omega_p^2 \left(1 + \frac{k^2}{\omega^2}\frac{T}{m_e}\right) \quad , \quad \Pi_{L,r} = \frac{K^2}{\omega^2}\omega_p^2 \left(1 + \frac{3k^2}{\omega^2}\frac{T}{m_e}\right) , \tag{2.8}$$

to first order in the small average electron velocities, where

$$\omega_p^2 = \frac{e^2 n_e}{m_e}\left(1 - \frac{5}{2}\frac{T}{m_e} + \mathcal{O}\left(\frac{T^2}{m_e^2}\right)\right) + \mathcal{O}\left(\frac{m_e}{m_n}\right) , \tag{2.9}$$

with T the temperature of the medium and n_e the electron number density. Figure 2 plots the corresponding dispersion relations. The essential physics is that the usual transverse modes are simply modified by the presence of a small effective plasma mass, whereas the longitudinal modes oscillate at an almost-fixed frequency set by the same plasma mass, propagating only through thermal diffusion effects.

This unusual dispersion relation for the longitudinal modes has the very important consequence that, for a light new particle of mass $m < \omega_p$, there is always a k where the dispersion relations of the new particle and the longitudinal photon cross. This means that the denominator in equation (2.6) can become small, allowing resonant production of the new state, as pointed out in the case of a dark photon by [12]. Resonant production from mixing with transverse photons is also possible, but only for m in a narrow range around ω_p.

The situation changes somewhat for relativistic or degenerate plasmas. As we increase the typical electron velocity, the propagation speed of the longitudinal mode increases, moving the point where the longitudinal dispersion relation crosses the lightcone to higher k. In the ultra-relativistic limit, both dispersion relations are always above the lightcone. However, the ratio of the cross-over point to the plasma frequency increases only logarithmically with the typical electron energy, so even for the highly relativistic plasma in a supernova core, cross-over still occurs at ω only a few times the temperature. Thus, there is still the possibility of resonant production for very light, weakly-coupled states through mixing with the longitudinal mode. Details are given in appendix C.

One point to note is, well below the light-cone, the photon self-energy will have more complicated behaviour, and the longitudinal propagator will generally have extra poles corresponding to ion acoustic oscillations etc. (cf. [13]). However, we are interested in the emission of weakly-coupled massive particles, so in the behaviour above the light-cone — in particular, resonant production can only occur for the longitudinal and transverse photon oscillations.

JHEP02(2017)033

For notational convenience, we define $m_T(K)^2 \equiv \Pi_{T,r}(K)$, $(K^2/\omega^2)\omega_L(K)^2 \equiv \Pi_{L,r}$; the longitudinal definition factors out the K^2/ω^2 dependence that appears automatically from the polarisation contractions. From the previous section, the width for transverse modes is $\Gamma_T(K) \simeq -\Pi_{T,i}/\omega$ in the dilute non-relativistic limit (in fact, as per [11], this is always true to good accuracy), and for longitudinal modes we write $-\Pi_{L,i} \equiv (K^2/\omega^2)\omega\sigma_L(K)$, where this equation defines $\sigma_L(K)$. In the non-relativistic case, $Z_L^{-1} = 1 - \frac{d\Pi_r}{d\omega^2} \simeq K^2/\omega_p^2$, so, the physical width of longitudinal plasmons is $\Gamma_L \simeq (Z_L/\omega_p)(-\Pi_{L,i}) = \sigma_L$.

2.2 Dark photons

Dark photons provide the simplest example of a new state mixing with SM photons. The physics in this case has been described in previous literature [6, 7], but we go over it here to show the similarity with other cases to follow, and since we will extend the dark photon constraints to include SN cooling and stellar trapping.

Suppose we have a new vector A', the 'dark photon', which couples to the SM EM current J,

$$\mathcal{L} \supset -\frac{1}{4}F^2 - \frac{1}{4}F'^2 + \frac{1}{2}m^2A'^2 + eJ(A + \epsilon A') \ . \tag{2.10}$$

Note that, after a field redefinition, this is equivalent to kinetic mixing $\mathcal{L} \supset -\frac{1}{4}F^2 - \frac{1}{4}F'^2 - \frac{\epsilon}{2}FF' + \frac{1}{2}m^2A'^2 + eJA$. We will assume that there are no additional BSM states at low energies, so that the mass m is a Stueckelberg mass (this is natural even with very small m, since J is a conserved current), rather than coming from a low-scale Higgs mechanism. Then, $\Pi^{XX} = \epsilon^2\Pi^{AA}$, $\Pi^{AX} = \epsilon\Pi^{AA}$, so writing $\Pi^{AA} \equiv \Pi = \Pi_r + i\Pi_i$,

$$-\ \mathrm{Im}(\omega_c^2) = \mathrm{Im}\left(\epsilon^2 m^2 \frac{\Pi}{\Pi - m^2}\right) + \mathcal{O}(\epsilon^4) = \epsilon^2 \frac{m^4(-\Pi_i)}{\Pi_i^2 + (\Pi_r - m^2)^2} + \mathcal{O}(\epsilon^4) \ . \tag{2.11}$$

In [6, 7], this result was obtained by going to the active/sterile basis, in which the sterile state couples to the SM only via its mass mixing with the active state. As per section 2, we then have no Π^{XX} 1PI contribution, but just the $(\Pi^{AX})^2/(\Pi^{AA} - m^2)$ term. The end result is, of course, independent of the basis chosen, as illustrated by our choice of the (vacuum) mass basis.

If the SM photon oscillations are weakly damped, $\Pi_i \ll \Pi_r$ (as is generally the case for the environments of interest here), we can split the production rate into four different contributions, with parametrically different properties:

- Continuum transverse production: the production of transverse weakly-coupled states has rate

$$\Gamma = \frac{1}{e^{\omega/T} - 1}\epsilon^2 m^4 \frac{\Gamma_T}{\omega^2\Gamma_T^2 + (m_T^2 - m^2)^2} \ . \tag{2.12}$$

  For $|m_T^2 - m^2| \gg \omega\Gamma_T$, i.e. off-resonance, this is

$$\Gamma \simeq \epsilon^2 \frac{m^4}{(m_T^2 - m^2)^2}\Gamma_{T,\mathrm{prod}} \ . \tag{2.13}$$

JHEP02(2017)033

For $m \gg m_T$, this is simply the 'naive' production rate $\epsilon^2 \Gamma_{T,\text{prod}}$, while for $m \ll m_T$, it is suppressed by m^4/m_T^4. In an active/sterile basis, this suppression comes from the propagator for the heavy active state [6].

- Resonant transverse production: for $|m_T^2 - m^2| < \omega \Gamma_T$, the production rate is[2]

$$\Gamma \simeq \frac{1}{e^{\omega/T} - 1} \epsilon^2 \frac{m^4}{\omega^2 \Gamma_T} \ . \tag{2.14}$$

If we consider production at a given frequency ω, then for a spatially-varying medium, there is some region for which the resonance condition holds. The size of this region will be set by $\sim \omega \Gamma_T / (\partial_x m_T^2)$, so the overall power emitted will be *independent* of Γ_T, in the small-width approximation. If we assume a spherically-symmetric medium, with m_T a function of ω, k, r, we have [12]

$$P = \int dr \, 4\pi r^2 \int \frac{d^3k}{(2\pi)^3} \frac{1}{e^{\omega/T} - 1} \epsilon^2 m^4 \frac{(-\Pi_i)}{(\Pi_i)^2 + (m_T^2 - m^2)^2} \tag{2.15}$$

$$\simeq \int d\omega \, 2k\omega \frac{1}{e^{\omega/T} - 1} \epsilon^2 m^4 \left(r^2 \left| \frac{\partial m_T^2}{\partial r} \right|^{-1} \right)_{r \text{ s.t. } m_T^2(\omega,k,r) = m^2} , \tag{2.16}$$

where the integral is over ω such that we match the resonance condition at some r.

- Continuum longitudinal production: the production of longitudinal weakly-coupled states has rate

$$\Gamma = \frac{1}{e^{\omega/T} - 1} \epsilon^2 m^2 \omega^2 \frac{\sigma_L}{\omega^2 \sigma_L^2 + (\omega^2 - \omega_L^2)^2} \ . \tag{2.17}$$

Off-resonance, this is

$$\Gamma \simeq \frac{1}{e^{\omega/T} - 1} \epsilon^2 \frac{m^2 \omega^2}{(\omega^2 - \omega_L^2)^2} \sigma_L \ . \tag{2.18}$$

As expected, the production rate is always suppressed by m^2 (since σ_L has already had the leading m^2 dependence factored out). Since the EM current is conserved, longitudinal emission is always suppressed by m^2, in vacuum and in medium [6].

- Resonant longitudinal production: for $|\omega^2 - \omega_L^2| < \omega \sigma_L$,[3]

$$\Gamma \simeq \frac{1}{e^{\omega/T} - 1} \epsilon^2 \frac{m^2}{\sigma_L} \ . \tag{2.19}$$

As noted in section 2.1, this differs from the resonant transverse case in that, if $m < \omega_L$, there is always a k such that the resonance condition holds. Therefore, we can find

[2] As mentioned in section 2, this expression holds if ϵ is small compared to $(\Pi - m^2)/\Pi$. In particular, at $\Pi_r = m^2$, if $\epsilon > \frac{1}{2}\omega\Gamma_T/m^2$, then to leading order in $\omega\Gamma_T/m^2$, we have $\Gamma \simeq (1/2)\Gamma_{T,\text{prod}}$, so the dark photon production rate never parametrically exceeds that for the SM photon.

[3] Analogously to transverse resonant production, this expression is valid for $\epsilon \ll \sigma_L/\omega$. If $\epsilon > (1/2)\sigma_L/\omega$, then to leading order in σ_L/ω, we have $\Gamma \simeq (1/2)(e^{\omega/T} - 1)^{-1}(m^2/\omega^2)\sigma_L$, so the resonant longitudinal production rate is always down by a factor of m^2/ω^2 relative to σ_L.

JHEP02(2017)033

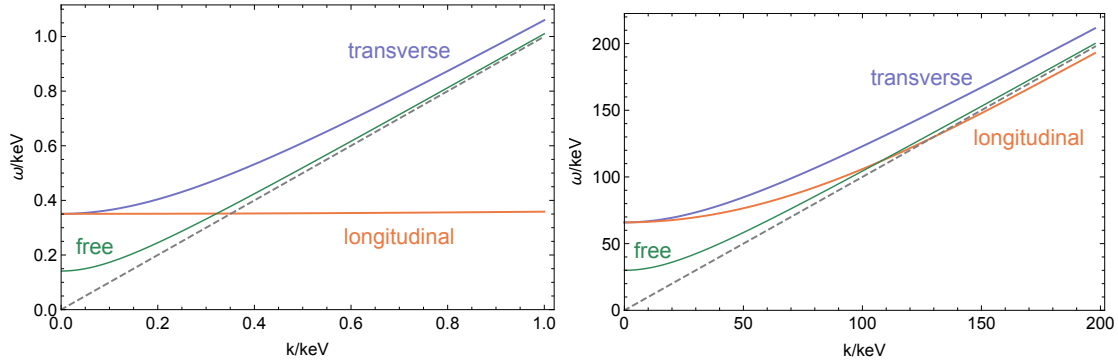

Figure 2. The photon dispersion relation in solar core plasma (left) and early universe plasma at $T = 1\,\mathrm{MeV}$ (right), showing non-relativistic and relativistic dispersion relations respectively. Blue lines show transverse dispersion relations, orange lines show longitudinal. For both plasmas, transverse and longitudinal oscillations are weakly damped, resulting in narrow resonances around the plotted frequencies. The grey dotted lines indicate the light cone. Green lines show example dispersion relations for weakly-coupled light particles ($m = 140\,\mathrm{eV}$ on left, $m = 30\,\mathrm{keV}$ on right). Since, as discussed in appendix C, the effects of increasing temperature and chemical potential once $T, \mu \gg m_e$ are almost degenerate, the right-hand plot is qualitatively similar to the shape of the dispersion relations in e.g. a SN core.

the emissivity at a given position, at leading order in the small-σ_L approximation, via

$$\frac{d\dot{N}_{\mathrm{prod}}}{dV} = \int \frac{d^3k}{(2\pi)^3}\Gamma_{\mathrm{prod}} = \int \frac{2k\omega d\omega}{(2\pi)^2}\frac{1}{e^{\omega/T}-1}\epsilon^2 m^2 \omega \frac{\omega\sigma_L}{(\omega\sigma_L)^2 + (\omega^2-\omega_L^2)^2} \tag{2.20}$$

$$\simeq \frac{1}{4\pi}\epsilon^2 m^2 k_{\omega_L}\omega_L \frac{1}{e^{\omega_L/T}-1}\left|1 - \frac{d\omega_L^2}{d\omega^2}\right|_{\omega_L}^{-1} . \tag{2.21}$$

As expected, at large masses $m \gg m_T, \omega_L$ we are in the kinetic theory regime for longitudinal and transverse emission. At masses small compared to the plasma frequencies, longitudinal production is dominant, being suppressed by m^2.

2.3 $B - L$ vector

As well as the electromagnetic current, there is another non-anomalous (assuming Dirac neutrinos) conserved current in the SM corresponding to $B - L$. A light vector coupling weakly to this current,

$$\mathcal{L} \supset -\frac{1}{4}X_{\mu\nu}X^{\mu\nu} + \frac{1}{2}m^2X^2 + gJ_{B-L}X\,, \tag{2.22}$$

where J_B is the SM $B - L$ current, is a popular candidate for new vector portal physics, e.g. [14]. Since $B - L$ does not have any mixed anomalies with the SM gauge groups, there are no order-g^2 production processes that are enhanced by powers of E^2/m^2, where E is the energy of the process. This means that a $B - L$ vector avoids the tight constraints, coming from high-energy experiments, that apply to vectors coupling to non-conserved currents.[4]

[4]If SM neutrinos are Majorana, then there is a $(B - L)^3$ anomaly — however, the cutoff scale implied by this anomaly is extremely high, and it is not a phenomenological concern.

JHEP02(2017)033

In this paper, we will suppose that the only light fermions coupling to X are those of the SM (the phenomenology we study is not significantly affected by whether neutrinos are Dirac or Majorana), and that X has a Stueckelberg mass.

In a medium consisting entirely of protons and electrons, the tree-level behaviour of a $B-L$ vector is exactly the same as for a dark photon. We therefore expect differences in thermal production of a light $B-L$ vector vs a dark photon to be driven by the neutron content of the medium.

For a dilute, non-relativistic plasma, the dominant contribution to the real parts of the X and A self-energies is from the electrons, and the imaginary parts are also dominated by emission from electrons (either electron-ion bremsstrahlung, or Compton scattering). So, we can write

$$\Pi_{r,i}^{XX} = \frac{g^2}{e^2}\Pi_{r,i}^{AA}(1+\alpha_{r,i})\,, \tag{2.23}$$

$$\Pi_{r,i}^{AX} = \frac{g}{e}\Pi_{r,i}^{AA}(1+\beta_{r,i})\,, \tag{2.24}$$

where α and β are suppressed by some function of the small parameter m_e/m_i. Then,

$$-\operatorname{Im}(\omega_c^2) = \frac{g^2/e^2}{\Pi_i^2+(\Pi_r-m^2)^2}(-\Pi_i)\Big(m^4(1+\alpha_i)+2m^2(\beta_r+\beta_i-\alpha_i)\Pi_r + (\Pi_r^2+\Pi_i^2)(\alpha_i-2\beta_i)\Big)\,, \tag{2.25}$$

where $\Pi \equiv \Pi^{AA}$ is the photon self-energy, and we have ignored higher order terms in α, β. As expected, the only part that is not α, β suppressed is the dark photon rate $m^4\Pi_i$, which will dominate at high masses, when the m^4 factor does not suppress it. In particular, we have the same resonant production contributions as for a dark photon, which were not visible in the 'kinetic theory' rate corresponding to $\Pi_i^{XX} = (g^2/e^2)\Pi_i^{AA}(1+\alpha_i)$.

The part of the production that is unsuppressed as $m \to 0$ depends on $\alpha_i - 2\beta_i + \mathcal{O}(\alpha^2, \beta^2)$ (for transverse emission; longitudinal emission is always suppressed by m^2). The α_i and β_i contribution from electron-ion bremsstrahlung are $\mathcal{O}(m_e/m_n)$ (arising from interference between emission from electrons and from ions), but these cancel at leading order, $\alpha_i - 2\beta_i = \mathcal{O}(m_e^2/m_n^2)$. This becomes clear if we go to a basis $\tilde{A} = A + (g/e)X$, $\tilde{X} = X - (g/e)A$, where $\tilde{X}$ only couples to neutrons — then,

$$\Pi_i^{\tilde{X}\tilde{X}} = \Pi_i^{XX} - 2(g/e)\Pi_i^{AX} + (g/e)^2\Pi_i^{AA} = (g/e)^2\Pi_i^{AA}(\alpha_i - 2\beta_i)\,, \tag{2.26}$$

and $\tilde{X}$ production in electron-ion bremsstrahlung is suppressed by m_e^2/m_n^2, since $\tilde{X}$ can only be emitted from the ion leg.

Compton production has no interference between emission from electrons and ions, and has $\alpha_i, \beta_i = \mathcal{O}(m_e^2/m_n^2)$ at leading order. The lowest-order in m_e/m_n contribution to m-independent production therefore comes from bremsstrahlung between different ion species, which is suppressed by $(m_e/m_n)^{3/2}$. At masses well below the plasma frequencies,

JHEP02(2017)033

this contribution will dominate the production, while at masses comparable or above, the dark-photon-like contribution is largest.[5]

The production of $B-L$ bosons in relativistic and/or degenerate plasmas is more complicated, and we leave it to future work.

2.4 $\phi\bar{f}f$ scalar

A scalar with renormalisable couplings to SM fermions,

$$\mathcal{L} \supset \frac{1}{2}(\partial_\mu\phi)^2 - \frac{1}{2}m^2\phi^2 + \sum_f g_{\phi f}\phi\bar{f}f\,, \tag{2.27}$$

in the low-energy theory, will also couple coherently to SM plasma oscillations. This action can arise, for example, from mixing with the SM Higgs.

The low-energy SM does not contain any scalar states, so vacuum ϕ-SM mixing is not possible. However, in a plasma, ϕ can mix with the in-medium 'longitudinal photon' mode.

For non-relativistic (relative to f) momentum transfers, $\bar{f}f \simeq \bar{f}\gamma^0 f$, so the contribution to the mixing self-energy from f will be

$$\Pi_\mu^{\phi A} \simeq \frac{g}{eQ_f}\Pi_{0\mu}^{AA} \quad \Rightarrow \quad \Pi_\mu^{\phi A}(\epsilon^L)^\mu \simeq \frac{g}{eQ_f}\frac{k}{\sqrt{K^2}}\Pi_L\,, \tag{2.28}$$

where Q_f is the EM charge of f. Thus, on mass-shell, there is a $\sim k/m$ enhancement over the longitudinal vector self-energy. As we will see below, this will translate into a different mass dependence of the overall production rate.

The damping rate for ϕ is, from equation (2.6), given by

$$\omega\Gamma_\phi = -\Pi_i^{\phi\phi} - \frac{\Pi_i^{AA}((\Pi_r^{A\phi})^2 - (\Pi_i^{A\phi})^2) - 2(\Pi_r^{AA} - m^2)\Pi_r^{A\phi}\Pi_i^{A\phi}}{(\Pi_i^{AA})^2 + (\Pi_r^{AA} - m^2)^2}\,, \tag{2.29}$$

Considering a $\phi\bar{e}e$ coupling as an example, this gives

$$\Gamma_\phi \simeq \frac{g^2}{e^2}k^2\omega\frac{\omega\sigma_L}{(\omega\sigma_L)^2 + (\omega^2 - \omega_p^2)^2}\,. \tag{2.30}$$

For $\omega_p < T$, this has a continuum contribution which is approximately the naive kinetic theory rate. If $m < \omega_p$, then there is also a resonant contribution, with emission at $\omega \simeq \omega_p$ at a rate

$$\frac{d\dot{N}_{\rm prod}}{dV} \simeq \frac{1}{4\pi}\frac{g^2}{e^2}k^2_{\omega_p}\omega_p^2\frac{1}{e^{\omega_p/T} - 1}\,. \tag{2.31}$$

[5] As discussed in appendix B, for sufficiently low-temperature plasmas, there is the additional complication that ion-ion bremsstrahlung is further suppressed by the ratio v_i/α, where $v_i \sim \sqrt{T/m_i}$ is the typical velocity of an ion, if this ratio is $\ll 1$. This occurs since the Coulomb interaction between ions is repulsive, and for low velocities, prevents them from getting within a de Broglie wavelength of each other, so limiting the accelerations they feel in the collision. For example, in the solar core, the velocity of protons is $\sim 10^{-3} \ll \alpha$. In this case, the ion-ion bremsstrahlung contribution is suppressed by $\sqrt{T}m_e^{3/2}/(m_n^2\alpha)$. Since $\sqrt{m_e/m_n} \sim 0.02$, there is the potential that m_e^2/m_n^2 contributions may be numerically important in such circumstances. For sufficiently dense plasmas, plasma screening will also be important, since the relevant ion separations during collisions is large due to Coulomb repulsion.

JHEP02(2017)033

Note that, unlike the case for a vector, this resonant contribution is not suppressed at small m. This resonant contribution may be larger or smaller than the continuum one, depending on the properties of the plasma. If $m \ll \omega_p < T$, then using $\omega_p^2 \simeq n_e e^2/m_e$, resonant emission gives

$$Q_{\rm res} \simeq 4\pi\alpha\alpha_\phi \frac{n_e^2 T}{m_e^2}\,, \tag{2.32}$$

while Compton and bremsstrahlung continuum emission give (from appendix B)

$$Q_{\rm Comp} \simeq \frac{8\alpha\alpha_\phi}{\pi} n_e \frac{T^4}{m_e^2} \quad , \quad Q_{\rm brem} \simeq 3\frac{n_e n_i}{m_e}\sqrt{\frac{T}{m_e}}\alpha^2\alpha_\phi Z_i^2\,, \tag{2.33}$$

so

$$\frac{Q_{\rm res}}{Q_{\rm Comp}} \simeq \frac{\pi^2}{2}\frac{n_e}{T^3} \quad , \quad \frac{Q_{\rm res}}{Q_{\rm brem}} \simeq \frac{4\pi}{3\alpha Z_i}\sqrt{\frac{T}{m_e}}\,. \tag{2.34}$$

We see that resonant production occurs at the same order in α as Compton production, but for a dense plasma where $n_e > T^3$, the resonant rate is larger. Bremsstrahlung production is suppressed by α compared to resonant production, but is enhanced by the inverse electron velocity. Since electron velocities in stellar cores can be almost relativistic, the resonant contribution can dominate, as we will see in section 3.4.

For relativistic / degenerate electrons, the calculations are slightly more complicated (see appendix D for details). However, the overall picture of resonant production being unsuppressed at small m, and being potentially larger than the continuum contribution, remains.

2.4.1 Coupling to nucleons

In the low-energy SM, we can consider a scalar coupling to nucleons, $\phi\bar{n}n$ and $\phi\bar{p}p$. For simplicity, we will take the n and p couplings to be equal here (this is approximately true for e.g. a Higgs portal scalar) — it is simple to extend to unequal couplings.

The real part of the mixing self-energy is, for non-relativistic nucleons,

$$\Pi_r^{\phi L} \simeq \sum_i e g Z_i A_i \frac{n_i}{m_i}\frac{k\sqrt{K^2}}{\omega^2} \equiv \frac{k\sqrt{K^2}}{\omega^2}\Omega_{eB}^2\,, \tag{2.35}$$

where Ω_{eB} is suppressed by $\mathcal{O}(m_e^2/m_n^2)$ relative to the plasma frequency. For a single species of ion, $\Omega_{eB}^2 \simeq (g/e)(m_e/m_n)\omega_p^2$. The damping rate is again given by equation (2.29), which simplifies to

$$\omega\Gamma_\phi \simeq (-\Pi_i^{\phi\phi}) + \frac{k^2}{\omega^2}\Omega_{eB}^2\left(\frac{2\omega\Sigma(\omega^2-\omega_L^2)+\omega\sigma_L\Omega_{eB}^2}{\omega^2\sigma_L^2+(\omega^2-\omega_L^2)^2}\right)\,, \tag{2.36}$$

where we have written $-\Pi_i^{\phi L} = k\sqrt{K^2}\Sigma/\omega$, and taking $\Omega_{eB}^4 \gg \omega^2\Sigma^2$. At $\omega \gg \omega_L$, the second term is suppressed by Ω_{eB}^2/ω^2, so production is dominated by $-\Pi_i^{\phi\phi}$, as expected. We also have a resonant contribution to the production rate, given by

$$\frac{d\dot{N}}{dV} \simeq \frac{1}{4\pi}\left(\frac{\omega_L}{m}\Pi_r^{\phi L}\right)^2 \frac{1}{e^{\omega_L/T}-1}\left|1-\frac{d\omega_L^2}{d\omega^2}\Big|_{\omega_L}\right|^{-1} \tag{2.37}$$

$$\simeq \frac{1}{4\pi}\frac{k_{\omega_p}^2}{\omega_p^2}\Omega_{eB}^4\frac{1}{e^{\omega_p/T}-1}\,. \tag{2.38}$$

JHEP02(2017)033

Both the resonant and non-resonant contributions will, in the case of equal couplings to protons and neutrons, be suppressed by m_e^2/m_n^2 relative to the $\phi\bar{e}e$ rates. As per the $B-L$ case, different ions have couplings almost proportional to their mass, resulting in a suppression of ion-ion bremsstrahlung, which would otherwise contribute at $(m_e/m_n)^{3/2}$. The emissivity relative to Compton and bremsstrahlung is parametrically the same as in the previous section.

3 Bounds on weakly-coupled bosons

We now evaluate some of the parametrically-new production rates discussed in the previous section for the physical plasmas inside stellar cores, and use these to estimate bounds on the masses and couplings of new bosons. We emphasise that our calculations should not be viewed as precise constraints, which would generally require a detailed numerical study of the observational data and stellar models. In addition, we do not aim to be comprehensive — we choose a number of new physics scenarios to illustrate our points, leaving many possibilities for future work.

Following [1], there are a number of scenarios in which we are particularly sensitive to novel energy losses from stars:

- *The Sun.* The Sun is not an exceptional star, but it is better-measured than others — in particular, it is the only star whose neutrino emission . With modern solar models, novel forms of energy loss can be constrained down to around 10% of the measured solar luminosity [7, 15] (global modelling using specific energy loss profiles can improve this limit to the few percent level [16]). This gives a limit on the average energy loss per unit mass of $\epsilon_{\rm new} \lesssim 0.2\,{\rm erg\,g^{-1}\,sec^{-1}}$. In the solar core, which is roughly half hydrogen and helium by mass,

$$T_{\rm core} \sim 1\,{\rm keV} \quad , \quad \rho_{\rm core} \sim 150\,{\rm g\,cm^{-3}} \quad , \quad \omega_p \sim 0.3\,{\rm keV}\ . \tag{3.1}$$

- *Red Giant (RG) cores just before helium ignition.* Red Giant cores before the onset of helium fusion are basically small, hot white dwarfs at the centre of the enormously-larger stellar atmosphere, whose electrons are mostly degenerate. Since the core is inert (not undergoing fusion), the main energy transfer process is energy loss by neutrino emission, $\epsilon_\nu \sim 4\,{\rm erg\,g^{-1}\,sec^{-1}}$. Novel energy loss processes can be constrained down to around this magnitude, $\epsilon_{\rm new} \lesssim 10\,{\rm erg\,g^{-1}\,sec^{-1}}$, since a more efficient loss process would delay the onset of helium ignition, in disagreement with observations that match stellar models (e.g. [17]). The conditions in the core just before helium ignition are approximately

$$T_{\rm core} \sim 10\,{\rm keV} \quad , \quad \rho_{\rm core} \sim 10^6\,{\rm g\,cm^{-3}} \quad , \quad \mu_e \sim 1.3 m_e \quad , \quad \omega_p \sim 20\,{\rm keV}\ . \tag{3.2}$$

- *Horizontal branch (HB) star cores during helium-burning.* During their helium-burning phase, the energy released by fusion puffs up the core of the star, lowering its density and making it non-degenerate. The power from helium fusion is

JHEP02(2017)033

$\epsilon_{3\alpha} \sim 80\,\mathrm{erg\,g^{-1}\,sec^{-1}}$. If there are additional energy-loss processes, these cause the core to contract, heating it up, enhancing the rate of the helium fusion, and so shortening the helium-burning lifetime of the star. This lifetime is measured to around the $\sim 10\%$ level, and agrees with standard stellar models, so novel energy losses are constrained to be $\epsilon_{\rm new} \lesssim 10\,\mathrm{erg\,g^{-1}\,sec^{-1}}$ constraints (e.g. [18]). The core properties are approximately,

$$T_{\rm core} \sim 10\,\mathrm{keV} \quad , \quad \rho_{\rm core} \sim 10^4\,\mathrm{g\,cm^{-3}} \quad , \quad \omega_p \sim 2\,\mathrm{keV}\ . \tag{3.3}$$

- *Core-collapse supernovae (SN).* In the first few seconds of a core-collapse supernova, the core is basically a very hot proto-neutron star, with degenerate electrons and almost-degenerate nucleons. It is sufficiently hot and dense to be optically thick even to neutrinos. The dominant energy loss mechanisms is via the outwards diffusion of neutrinos, which occurs over a $\sim 10\,\mathrm{s}$ timescale — the resulting neutrino burst was measured for SN1987A [1], with properties that agreed with SN model predictions. In order for a new energy-loss mechanism not to have disrupted the SN1987A neutrino burst, the averaged energy loss rate would have to have been less than that from the neutrinos, $\epsilon_{\rm new} \lesssim 10^{19}\,\mathrm{erg\,g^{-1}\,sec^{-1}}$ [1].

$$T_{\rm core} \sim 30 - 60\,\mathrm{MeV}\,, \quad \rho_{\rm core} \sim 3 \times 10^{14}\,\mathrm{g\,cm^{-3}}\,, \quad \mu_e \sim 350\,\mathrm{MeV}\,, \quad \omega_p \sim 20\,\mathrm{MeV}\ . \tag{3.4}$$

  As we will see, for particle emission processes that do not depend on high powers of the temperature or density, stellar limits are generally more constraining than SN limits for masses $\lesssim 50\,\mathrm{keV}$. However, SN limits apply up to masses $\sim 100\,\mathrm{MeV}$.

  It should be emphasised that there is still significant uncertainty regarding the behaviour of core-collapse supernovae [19], with conflicting models in the literature of even the very basic energy source involved [20]. As a result, SN constraints on new light particles should be viewed as order-of-magnitude estimates at best.

- *Very degenerate stellar remnants: white dwarfs (WDs) and neutron stars (NSs).* These have the desirable properties of fairly inefficient SM energy-loss mechanisms (either neutrino emission, or surface photon emission), as well as reasonable temperature and high density compared to the aforementioned stellar core situations. However, the emission of new particles in scattering process is generally highly suppressed by Pauli-blocking. As a result, WDs can only impose similar constraints to those from stars in some cases, while NSs do not seem to be competitive [1]. For resonant emission, the situation is ever worse: since these highly degenerate systems have plasma frequencies $m_T, \omega_L \gg T$, emission at resonant frequencies is heavily Boltzmann-suppressed, so is never significant.

JHEP02(2017)033

3.1 Emission and trapping

The production calculations in section 2 looked at the production rate per unit volume for a weakly-coupled in-medium mode, assuming a uniform, time-independent thermal medium. For stellar cooling bounds, we are interested in the energy flux that escapes the core — that is, in the energy transport between regions with different medium properties. However, as long as medium properties vary slowly enough, then a weakly-coupled mode emitted from one region will propagate adiabatically into the weakly-coupled mode for the new region (if the weakly-coupled and strongly-coupled modes go through level-crossing during the propagation, there will be resonant conversion, which needs to be taken into account).

Consequently, as long as absorption (and resonant conversion) during the course of the propagation is small, almost all of the energy emitted in weakly-coupled excitations at the centre is transported to weakly-coupled excitations further out. When the whole star is optically thin to weakly-coupled excitations, energy is lost to infinity, and the total energy loss rate is obtained by integrating over the per-volume production rate.

If weakly-coupled excitations are not able to free-stream through the whole star, then they contribute to energy transport within the star, and let the outer layers of the star lose energy to infinity (once the optical depth becomes low). Since our models of stellar structure fit observations fairly well, there is generally no room for a whole additional degree of freedom to contribute to radiative heat transport, unless that degree of freedom is heavy enough that its Boltzmann-suppressed abundance is too small to contribute significantly [1]. We will see in sections 3.3 and 3.4 how this opens up some extra parameter space at high masses and couplings, for stellar bounds on new particles. As discussed in section 3.2.1, numerical simulations of supernovae also seem to indicate that energy transport by particles with mean free path significantly larger than that of neutrinos is not compatible with SN1987A observations, allowing similar energy-transport bounds to be placed.

3.2 Dark photon production in supernovae

The uncertainty surrounding the behaviour of core-collapse supernovae is an obstacle to using detailed explosion models to constrain new physics. As mentioned in the Introduction, our focus in this paper is on highlighting the physical consequences of plasma effects, rather than attempting comprehensive and robust stellar modelling. Accordingly, we adopt a single representative supernova model (from [21], which is similar to others found in the literature, see e.g. the review [22]), and impose the simple 'Raffelt bound' approximation on the energy loss from new particles. That is, we demand that the average energy loss per unit mass from the core via new particles is $\lesssim 10^{19}\,\mathrm{erg\,g^{-1}\,sec^{-1}}$ [1] — in a variety of simulations, this is within a factor ~ 10 of the critical energy loss rate at which the neutrino signal would be detectably modified [23]. Thus, the constraints we derive should not be considered as robust parameter space exclusions. However, as we will see, plasma mixing can lead to orders-of-magnitude differences in the production and absorption rates, compared to a kinetic theory calculation [4, 5, 9]. Such effects will therefore be very important to include in any eventual robust study, and our calculations indicate how such exclusion bounds will vary with dark photon mass.

JHEP02(2017)033

In the supernova environment, the real part of the photon self-energy is dominantly generated by electrons,[6] the form of which is discussed in section 2.1 and appendix C. The imaginary parts of the photon self energy gets contributions from various processes, and the large rate of nucleon-nucleon interactions means that neutron-proton bremsstrahlung is dominant. Following [5], we can approximate the bremsstrahlung production rate by relating it to proton-neutron scattering data, using the soft approximation for photon emission. This is only strictly correct in the limit that the emitted energy is small compared to the kinetic energy of the collision, but from [5], we expect that the overall error from this approximation will be comparable to the other uncertainties in our calculation. Further details are given in appendix F. For some supernova models, the SM photon oscillations may become broad resonances in the supernova core, in which case the split of dark photon production into continuum and resonant contributions loses its applicability.

In figure 3 we plot the bounds obtained for our SN model after including the mixing effects discussed in section 2.2 — the bounds that would be obtained neglecting such effects are also shown.[7] At masses below the typical plasma frequency, transverse continuum emission has the expected $\epsilon \sim 1/m^2$ scaling. Meanwhile, longitudinal continuum and resonant emission both scale as $\epsilon \sim 1/m$. At masses around the plasma frequency, resonant transverse emission is possible, and leads to a stronger constraint, while at higher masses continuum emission of longitudinal and transverse modes is close to the kinetic theory prediction.

For dark photon masses below approximately 0.1 MeV, bounds from stellar cooling become dominant, also shown in figure 3. Production in these environments is less suppressed since the plasma frequency is lower, and they are better modelled and measured than supernovae. For masses below $2m_e$ there are also strong constraints from cosmology — a small dark photon abundance is produced in the early universe, which then decays to three photons, which would be visible in the observed gamma ray background [8] (or, for sufficiently early decays, through effects on the CMB or BBN). Such constraints could be relaxed by allowing the dark photon to decay to light hidden sector states, though the viability of this possibility is model dependent. There are also cosmological constraints for $m > 2m_e$ mixings [26, 27], but these constrain significantly smaller mixings than the supernova cooling limits.

In addition to affecting the neutrino signal through energy loss from the SN core, new particles that decay to SM could have other experimentally-visible signatures in SN. [9] considers some of these signatures for a dark photon, including gamma radiation from the injection of e^+e^- pairs when dark photons decay slightly outside the star. However, they use the kinetic theory calculation for dark photon production, so their constraints would need re-calculating with the correct production and absorption rates. We leave this to future work.

[6] The proton contribution is suppressed, since protons are non-relativistic in the SN; the neutron-neutron contribution vanishes in the limit that neutrons can be treated as free, and remains suppressed after allowing for interactions in a typical SN environment [24].

[7] Our results are compatible with [25], which considers a range of SN profiles, finding roughly an order of magnitude variation in the bounds obtained. Our SN profile is close to those denoted "Fischer" in [25], and leads to similar constraints.

JHEP02(2017)033

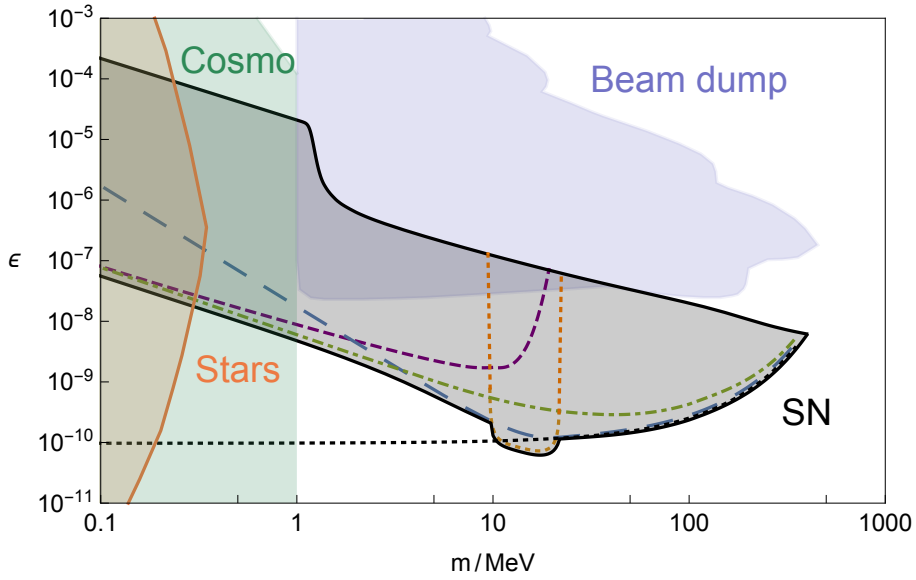

Figure 3. Constraints on dark photon couplings from SN1987A observations, for a particular supernova model as described in the text. The solid black region indicates the overall constraints. Subcomponents of the total emission are indicated; dotted (orange), resonant transverse emission, long-dashed (blue), continuum transverse emission, dot-dashed (green), continuum longitudinal emission, dashed (purple), resonant longitudinal emission. The limit on ϵ that would be obtained from a kinetic theory calculation is shown in dotted black. Assuming purely SM decays of the dark photon, the parameter space above the shaded region is not excluded by the energy loss constraint we impose because of absorption and/or decays to electron-positron pairs (at masses $\gtrsim 2\,\mathrm{MeV}$) (although energy transport via the dark photon may mean that the neutrino signal is still observably shortened — see section 3.2.1). Under the same assumption, beam dump experiments exclude the region shaded in blue [28]. The orange shaded region is excluded by stellar cooling bounds [6, 7] (where we have also incorporated the effects of trapping inside the star, as per section 3.1), while in models without hidden sector decays masses below $\sim$ MeV will be constrained by cosmological observations (green, [8] — the small gap at large mixing will very probably be closed by beam dump experiments such as [29]). It should be stressed that models of core-collapse supernovae are very uncertain, and limits such as those derived here, which assume a particular SN model [21], should be treated as order-of-magnitude estimates at best.

3.2.1 Trapping and decay

If ϵ is large enough, then for the SN core there is some (frequency-dependent) radius within which dark photon radiation gets reprocessed into nearly black-body radiation.[8] The core will then lose energy, at a given frequency, approximately like a black-body sphere of that radius (with surface temperature the medium temperature at that radius), along with

[8]Along a given 'line of sight' out of the core, the occupation number f of a weakly-coupled state propagating in that direction will evolve as $v\,df/dx = -f\Gamma_{\mathrm{abs}} + (1+f)\Gamma_{\mathrm{prod}} = \Gamma_{\mathrm{prod}} - f\Gamma_{\mathrm{damp}}$ where v is the velocity of the weakly-coupled state. So, for intervals over which the 'damping depth' $\tau_d \equiv \int dx\,\Gamma_{\mathrm{damp}}/v$ is large, the occupation number converges to the black-body value $f_B = \Gamma_{\mathrm{prod}}/\Gamma_{\mathrm{damp}}$, while for intervals over which $\tau_d \ll 1$, we simply integrate the production rate along the line. For frequencies $\omega \gtrsim T$, we have $\Gamma_{\mathrm{damp}} \simeq \Gamma_{\mathrm{abs}}$, so the damping depth is approximately the optical depth. For $\omega \ll T$, $\Gamma_{\mathrm{damp}} \simeq (\omega/T)\Gamma_{\mathrm{abs}}$, so the damping depth is significantly smaller than the optical depth.

JHEP02(2017)033

volume emission from the region outside. If these black-body radii are large enough, and correspond to small enough medium temperatures, then the overall energy loss rate via the dark photon will become small compared to the neutrino rate.

We make the assumption that, to significantly affect the neutrino signals, there needs to be energy loss greater than the Raffelt bound from the part of the core at temperature $\gtrsim 1.5\,\mathrm{MeV}$ [5]. As per section 3.1, it is likely that provided the dark photon mean free path is greater than of neutrinos in the core, the increased efficiency of energy transport would observably shorten the neutrino signal [21, 30, 31]. Imposing this condition would allow dark photon coupling roughly an order of magnitude stronger than those constrained by the energy loss bound to be ruled out; however, detailed simulations would be required to obtain quantiative bounds. Since such strong couplings are already ruled out by beam dump experiments, we only show the energy loss bounds in figure 3.

For the supernova profile we use, the $T = 1.5\,\mathrm{MeV}$ boundary is at a radius of approximately 14.5 km, by which point the electron chemical potential has dropped significantly, to $\sim$ MeV. This corresponds to the typical region from which neutrinos can free stream out of the supernova. Note however, it might be that energy has to escape to much larger distances, before the dark photons suppress neutrino productions significantly [25].

Up to such radii, continuum absorption of dark photons is dominated by inverse proton-neutron bremsstrahlung, expressions for which are given in appendix F (at much larger radii, inverse Compton scattering off electrons may become important). The ω^{-3} dependence of the bremsstrahlung absorption rate means that low-frequency dark photons are trapped more efficiently than higher-frequency ones, and so the frequency dependence of the effective black-body radius is important. For dark photon masses $\gtrsim 100\,\mathrm{keV}$, continuum absorption of transverse dark photons is more efficient than longitudinal continuum absorption, because of the small plasma frequency in the outer part of the supernova core. For small enough dark photon masses, transverse absorption will be suppressed by the expected m^4/ω_p^4 factor, so transverse photons will escape most easily, but such small masses are constrained by stellar cooling observations. Longitudinal dark photons can be resonantly absorbed if there is a shell where the supernova conditions are such that $\left|\omega^2 - \omega_L^2\right| < \omega\sigma_L$ is satisfied, and if present this shell is typically optically thick for ϵ at the trapping bound. Meanwhile, resonant reabsorption of transverse modes occurs for dark photon masses around the typical plasma frequencies.

If the dark photons decay to electrons and positrons before escaping the neutrino emission region, this will also prevent efficient energy loss (although as for absorption, the neutrino signal may still be observably shortened). In the centre of the supernova, decay to electrons is blocked by the high chemical potential, unless the mass of the dark photon is above twice the effective electron mass, $m_{\mathrm{eff}} \simeq 15\,\mathrm{MeV}$. However, towards the outside, the chemical potential drops sharply, and the effective electron mass is close to its vacuum value. In appendix E we give explicit formula for the decay rate.

The effect on the allowed values of ϵ is plotted in figure 3. For dark photon masses $m \gtrsim 2m_e$, decays dominate the absorption, although this is sensitive to the details of the supernova profile. If the dark photon can decay to lighter hidden sector states, which interact sufficiently weakly with the supernova medium that they can escape, decays and

JHEP02(2017)033

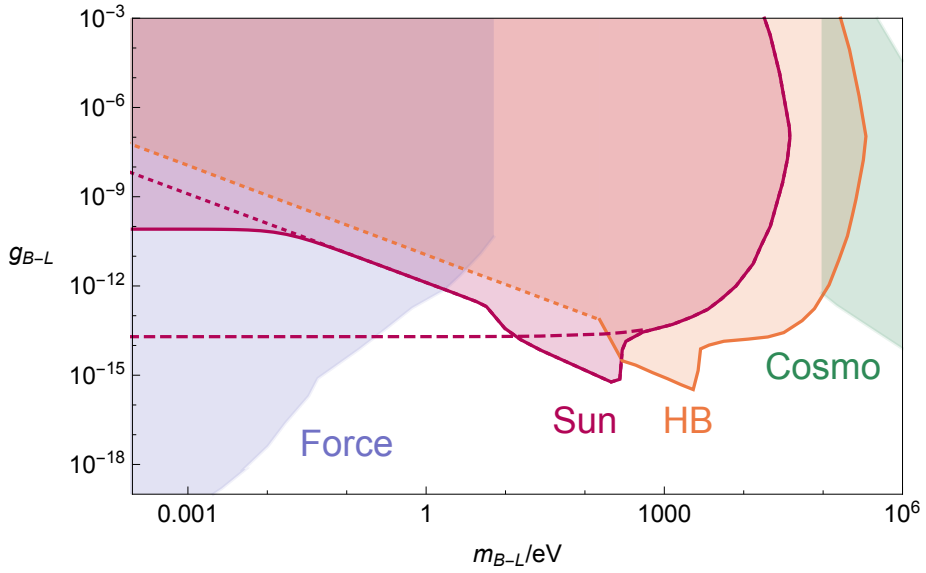

Figure 4. Constraints on the coupling of a $B - L$ vector, from force tests (blue, [32–36]), stellar cooling (see text) and cosmological observations (green, [8]). The solar bounds (red) take into account the mass-independent part of the production rate discussed in section 2.3, shown by the solid line — the dotted line shows the constraints that would arise if the coupling to neutrons were neglected. As explained in the text, the value of the mass-independent contribution to the production shown here is an order-of-magnitude estimate. The HB star bounds (orange) do not take into account the coupling to neutrons, so are shown dotted at low masses, where the neutron contribution will be important. The dashed red line indicates the bounds that would be obtained from a naive 'kinetic theory' calculation, which ignored in-medium mixing effects.

absorption would be reduced and larger values of ϵ constrained. This could also relax limits from beam dump experiments, and, as mentioned, alter cosmological constraints. The interplay of these effects would be interesting to study in the future.

3.3 $B - L$ vector bounds

From section 2.3, B-L production in a dilute, non-relativistic plasma should be well-approximated by the dark photon production rate, plus a mass-independent production rate that is suppressed by at least $(m_e/m_n)^{3/2}$. As discussed in footnote 5, the proton velocity in the Sun is small enough that the extra $\sim v/\alpha$ suppression of ion-ion bremsstrahlung makes it numerically comparable to the $(m_e/m_n)^2$ contribution from electron-ion bremsstrahlung. The plasma screening length inside the solar core is also small enough that it may affect the ion-ion bremsstrahlung calculation. We have not treated all of these contributions precisely, so our numerical value for the mass-independent production rate should be treated as an order-of-magnitude estimate. For the Sun, where the core is roughly half hydrogen and half ^{4}He by mass, we obtain the bounds shown in in figure 4. There will also be low-mass bounds from HB and RG stars — however, since these are unlikely to rule out significant areas of parameter space not already constrained by force bounds, we restrict ourselves to the solar calculation as an illustration. Figure 4 also shows the trapping bounds for

JHEP02(2017)033

emission from the Sun and from HB stars, as discussed in section 3.1 — these constraints translate directly to the dark photon case, in the high-mass region.

Comparing to the existing literature, stellar bounds on massive $B-L$ vectors have been considered in [2, 37, 38]. [2] performs the naive kinetic theory calculation, ignoring plasma mixing effects. [37, 38] treat the production of on-shell vectors as being the same as for dark photons, which ignores the mass-independent production rate from non-hydrogen nuclei calculated in section 2.3. [37, 38] also claim that there is a strong bound from the enhanced emission of SM neutrinos. However, the $B-L$ mediated emission of neutrinos has rate $\sim g_{B-L}^4$, which is extremely small, while the rates in the aforementioned papers appear to be $\sim g_{B-L}^2$.

Figure 4 also shows the bounds on a light $B-L$ vector from fifth-force tests [32–36], which are more constraining than stellar cooling bounds for masses $\lesssim$ eV. It also indicates the cosmological bounds arising from late-time three-photon decays of a $B-L$ population, produced in the early-universe plasma. These can be derived directly from the dark photon bounds [8], since the dominant contribution to early-universe production happens around electron-positron freeze-out, when only the electron coupling is important. The cosmological bounds depend on the $B-L$ vector not having hidden sector decays. Another possible probe of $B-L$ vectors or dark photons would be the direct detection of weakly-coupled states emitted from the Sun, in dark matter experiments on Earth [39, 40].

As is the case for dark photons, there will also be supernova cooling bounds on $B-L$ vectors of mass $\lesssim$ a few hundred MeV. Since neutrons play an important role in a supernova core, we expect the constraints to be rather different from those in the dark photon case. We leave an analysis of these to future work.

The importance of plasma mixing effects does not just apply to $B-L$ vectors or dark photons, but to any new vector coupling to the SM. For example, the bounds on a new vector coupling to baryon number derived in [3, 5] did not consider mixing effects, so would need to recomputed with those taken into account. Again, we would expect kinetic-theory-like emission at energies above the plasma frequencies, some enhancement from resonant emission at masses around the plasma frequencies, and then some suppression due to interference effects at lower masses.

3.4 $\phi \bar{f} f$ scalar bounds

As discussed in section 2.4, the production rate for a scalar that couples coherently to SM plasmons has a resonant contribution for $m < \omega_p$, and a continuum contribution that is roughly similar to the naive kinetic theory value. The resonant contribution is lower-order in α than the continuum bremsstrahlung rate, and is expected to be larger for plasmas with large electron velocities.

3.4.1 Coupling to electrons

Using the non-relativistic resonant production rate from equation (2.31), and taking a sample HB star model from [41], imposing the rough constraint $\epsilon \lesssim 10\,\mathrm{erg\,g^{-1}\,sec^{-1}}$ gives

$$\alpha_{\phi \bar{e} e} \lesssim 8 \times 10^{-31}\,, \tag{3.5}$$

JHEP02(2017)033

for $m \ll$ keV, where $\alpha_{\phi\bar{e}e} \equiv g^2_{\phi\bar{e}e}/(4\pi)$. For comparison, the kinetic theory production rate would give $\alpha_{\phi\bar{e}e} \lesssim 1.5 \times 10^{-29}$ (in agreement with the estimate from [1]). Since the continuum production is dominated by ^{4}He bremsstrahlung, we expect the ratio of resonant to transverse power per volume to be given by equation (2.34),

$$\frac{Q_{\rm res}}{Q_{\rm brem}} \simeq \frac{4\pi}{3\alpha Z_i}\sqrt{\frac{T}{m_e}} = 37\sqrt{\frac{T}{10^8\,\mathrm{K}}}\,, \tag{3.6}$$

Since our HB model has $\langle\sqrt{T/10^8\,\mathrm{K}}\rangle \simeq 0.5$ averaged over the core, this gives the correct ratio of ~ 20 between the continuum and resonant constraints.

For a RG core, where the electrons are degenerate, we can use the formulae from appendix D to calculate the resonant production rate. Using a sample RG core model from the MESA package [42], and imposing $\epsilon \lesssim 10\,\mathrm{erg\,g^{-1}\,sec^{-1}}$, we obtain

$$\alpha_{\phi\bar{e}e} \lesssim 4 \times 10^{-32}\,, \tag{3.7}$$

for $m \ll 10\,$keV. Calculating the continuum production rate in this case is more difficult, due to the electron degeneracy, but we expect resonant production to dominate at small masses. To summarise, for small scalar masses, we have the constraints

$$\alpha_{\phi\bar{e}e} \lesssim \begin{cases} 1.5 \times 10^{-29} & \text{(HB continuum production)} \\ 8 \times 10^{-31} & \text{(HB star resonant production)} \\ 4 \times 10^{-32} & \text{(RG core resonant production)}\,. \end{cases} \tag{3.8}$$

The corresponding mass-dependent constraints are shown in figure 5.

A calculation similar to that performed in section 3.2 could be done to find SN bounds on the $\phi\bar{e}e$ coupling. We are not aware of any existing calculation in the literature, and we leave such a treatment to future work.

3.4.2 Coupling to nuclei

Performing the analogous calculations for a scalar coupling to nucleons, assuming that we couple equally to protons and neutrons, we obtain

$$\alpha_{\phi\bar{N}N} \lesssim \begin{cases} 5 \times 10^{-23} & \text{(HB continuum production)} \\ 3 \times 10^{-24} & \text{(HB star resonant production)} \\ 1 \times 10^{-25} & \text{(RG core resonant production)}\,, \end{cases} \tag{3.9}$$

for small scalar masses (note that our continuum production bound is slightly tighter than that given in [1], since only Compton scattering is considered there, and electron-ion bremsstrahlung production is dominant for low-mass scalars). We again obtain a ratio of ~ 20 between resonant and continuum production for HB stars, and a significantly stronger bound from RGs. Figure 5 shows the mass-dependent bounds.

JHEP02(2017)033

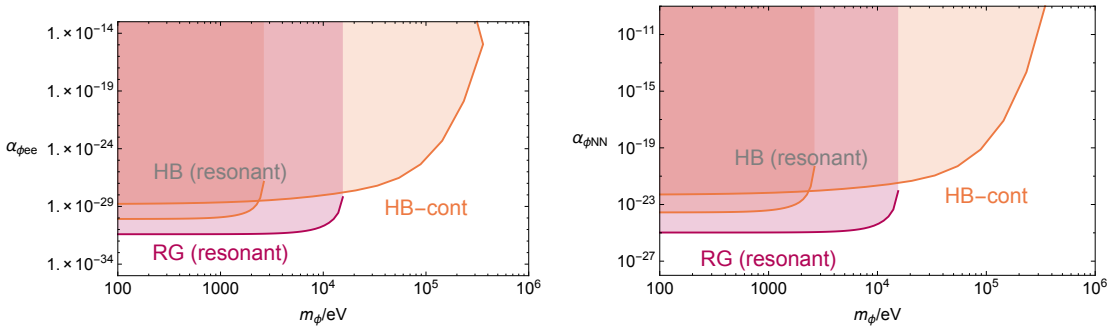

Figure 5. Stellar cooling constraints on a scalar ϕ with a $\phi\bar{e}e$ coupling (left), or a $\phi\bar{N}N$ coupling to nucleons (right), where we assume that ϕ couples equally to protons and nucleons. Both the continuum and resonant limits continue to very small ϕ masses. Continuum production of ϕ in HB stars gives approximately the same energy loss as a naive kinetic theory calculation. There will also be continuum production from RG cores, but this is more complicated to calculate due to electron degeneracy, so we leave it to future work (we expect it to be sub-dominant to resonant production at small masses). At high masses and couplings, the contribution of ϕ to energy transport in the star becomes small enough that it is not constrained by observations (section 3.1), as shown the in left-hand plot (the trapping constraints occur at larger α than shown in the right-hand plot). In a full model, there will also be other constraints on these parameter spaces, including force bounds and cosmological observations (for example, figure 6 shows the constraints on a Higgs portal scalar model).

3.4.3 Higgs portal scalar

The $|H|^2$ operator is the unique renormalisable portal through which a neutral scalar can be coupled to the SM. In the low-energy SM, its effects can be parameterised by a mixing angle $\sin\theta$, with the scalar ϕ coupling to fermions as $(m_f/v)\sin\theta\phi\bar{f}f$, where $v \simeq 246\,\text{GeV}$ is the electroweak vev. This gives a coupling to electrons of $g_{\phi\bar{e}e} = (m_e/v)\sin\theta = 2\times10^{-6}\sin\theta$, and a coupling to nucleons of $g_{\phi\bar{N}N} \simeq 8\times10^{-4}\sin\theta$ [43] (this is approximately the same for neutrons and protons, since most of the coupling does not come from the valence quarks). Since $g_{\phi\bar{e}e}/g_{\phi\bar{N}N} \simeq 2\times10^{-3} > m_e/m_n \simeq 5\times10^{-4}$ — as expected, since most of the nucleon mass comes from QCD, not from the Higgs VEV — the $\phi\bar{e}e$ coupling dominates the ϕ production rate in stellar cores, resulting in the stellar cooling bounds shown in figure 6. An interesting point is that the enhanced stellar cooling constraints are able to probe potentially natural parameter space for a Higgs portal scalar, as indicated in figure 6.

Comparing these to other constraints, the stellar cooling bounds are more stringent than fifth-force constraints at masses $\gtrsim 0.2\,\text{eV}$. Having a UV complete model also enables us to consistently compare the stellar bounds to cosmological constraints (assuming that the universe was reheated above the electroweak scale, and that there was no cosmologically-important new physics below the EW scale). [44] estimates the early-universe ϕ production, which is dominated by temperatures around the electroweak scale, and then constrains the later energy injection from $\phi \to \gamma\gamma$ decays. This gives the bounds shown in figure 6, indicating that the stellar bounds are probably the most constraining up to masses $\sim 10\,\text{keV}$. We leave an improved calculation of early-universe ϕ production, incorporating plasma effects, to future work. It would also be interesting to calculate the minimal bounds, assuming only that the reheating temperature is $\gtrsim$ MeV.

JHEP02(2017)033

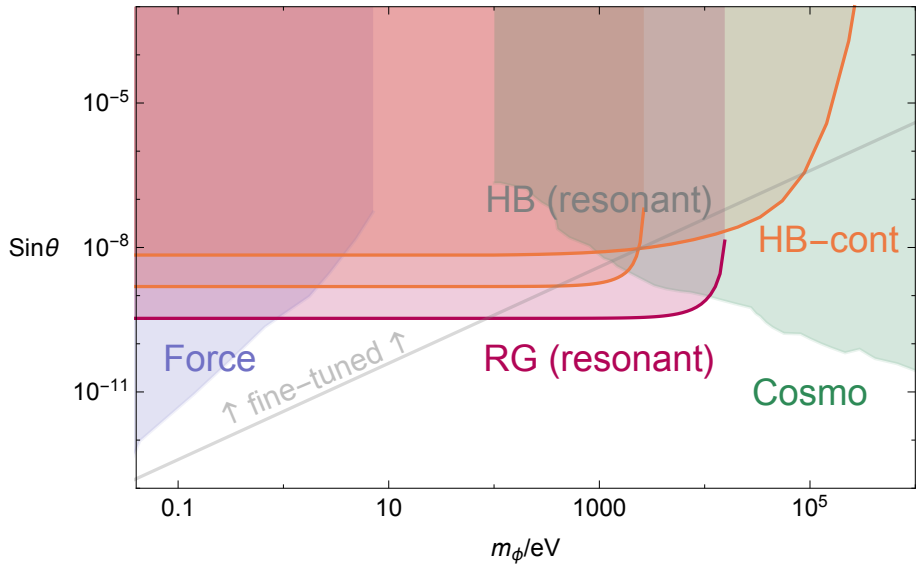

Figure 6. Constraints on a scalar ϕ with a Higgs portal coupling (section 3.4.3), where $\sin\theta$ is the mixing with the SM Higgs. Force bounds [32–36] are in blue, stellar cooling bounds (see text) in red and orange, and cosmological constraints in green. The latter arise from a freeze-in relic abundance decaying around the present day, contributing to the observed photon background [44] (we show these bounds as extending up to couplings at which ϕ would decay at BBN time, though it would require further work to verify whether the constraints are valid there). Since most of the nucleon mass comes from QCD, rather than from the Higgs VEV, the ratio of nucleon to electron ϕ couplings is smaller than the nucleon-electron mass ratio. The electron coupling therefore dominates the ϕ-SM mixing, and thus the resonant ϕ production, as well as dominating the continuum production. The stellar cooling bounds are therefore the appropriate rescaling of the $\phi\bar{e}e$ bounds show in the left-hand panel of figure 5, and likewise continue to very small ϕ masses. The grey line shows the approximate fine-tuning bound $\sin\theta \lesssim m_\phi/v_{\rm EW}$ [45], demonstrating that our new stellar constraints are able to probe natural parameter space.

4 Discussion

In this work, we have demonstrated how, in the medium of a SM thermal bath, plasma effects can introduce an effective in-medium mixing between hypothetical new, weakly-coupled bosons and SM photons (if the new bosons couple coherently to SM plasma oscillations). Such mixing affects the production of the new bosons by allowing resonant production from SM photons, and also by allowing cancellation between new boson and photon emission amplitudes. This can make a parametric difference to production rates from plasmas where chemical potentials are important, such as stellar cores.

Dark photons provide the simplest example of these effects, which were treated correctly in some, though not all, of the previous literature. In section 3.2, we estimate the production of dark photons in core-collapse supernovae, previous calculations of which ignored mixing effects [4, 5, 9], and use this to place new constraints in the mass-mixing parameter space. Note that there are very probably extra constraints one could place from arguments beyond simple energy-loss-from-core [9], but we leave those to future work.

JHEP02(2017)033

We also update the stellar-cooling constraints to include trapping effects, for heavy and more-strongly-coupled dark photons.

Extending these results to other types of new vectors, we illustrate the effects in the case of a weakly-coupled $B-L$ vector. In section 3.3, we estimate $B-L$ stellar cooling bounds, correcting previous literature [2, 37, 38]. Weakly-coupled scalars can have an in-medium mixing with longitudinal photon oscillations. Resonant production of such scalars, in particular from the cores of RG stars, places significantly stronger constraints (section 3.4, figure 6) than previous calculations which ignored mixing effects. Other BSM particle candidates which could result in similar effects include vectors coupling to other SM current (though the non-conservation of these currents generally leads to strong constraints from high-energy experiments), other forms of scalar coupling, and higher-spin new particles (e.g. KK gravitons, as considered in [23]). We leave the calculation of such constraints to future work.

Since the low-energy SM preserves parity, axion-like particles do not mix with SM plasma excitations, up to effects suppressed by weak-scale masses. However, if there is a parity-violating background, such as a strong magnetic field, then plasma mixing effects may become important. Nevertheless, even for a supernova, which may have magnetic fields of order 10^{15} Gauss [46], rough estimates indicate that this effect will be sub-leading. The temperature in a SN core is also hot enough that mixing with pions will have a small effect, but the pion mass is large enough that this will also be sub-dominant to other processes.

Up until the recombination era (i.e. for temperatures $\gtrsim$ eV), the universe was a hot, basically homogeneous plasma, so our calculations of the production rate for light, weakly coupled particles from this plasma will apply. Such production can also, with some assumptions, be used to place constraints on the properties of light particles, and as per stellar cooling calculations, plasma effects may make an important difference. For example, the cosmological bounds on a light $B-L$ vector, as shown in figure 4, are from the late-time decay of a small relic $B-L$ abundance produced in the early universe, and at the masses indicated, this abundance is dominated by resonant production around electron-positron freeze-out [8]. However, the early universe differs from stellar cores in a number of ways — chemical potentials were probably very small, and variation was in time instead of space — so the new particle candidates for which plasma effects make an important difference to observable quantities are not necessarily the same as those for stellar cooling bounds. We leave calculations of plasma effects on such early universe physics to future work.[9]

'Medium effects' of the kind discussed in this paper are sometimes important in laboratory searches for BSM particles, particularly at very low masses (e.g. [47, 48]). If we are interested in particle masses well above the plasma frequency of bulk materials, $\sim$ eV, then bulk medium effects will be negligible. For particle production in processes involving nuclei, the effective 'plasma frequency' of the nuclear 'medium', which we expect to be $\sim 10\,\mathrm{MeV}$, may be significant. For example, the beam dump constraints on dark pho-

[9]There have been a number of papers investigating the early-universe cosmology of dark photons, including [8, 26, 27].

JHEP02(2017)033

tons shown in figure 3 come from the production of dark photons in high-energy collisions between electrons/protons and target nuclei. However, the very small size of nuclei introduces important differences with respect to the stellar production case; in particular, nuclei are optically thin to SM photons as well as to dark photons. Thus, the previous arguments about only needing to consider the production of the weakly-coupled in-medium state will not hold. Further work would be required to calculate the nuclear medium effects on particle production in experiments such as beam dumps.

An important point is that the mixing effects giving rise to resonant production etc are better viewed as 'plasma' effects, rather than 'thermal' ones. In particular, although we have used the apparatus of thermal field theory to calculate them, they will also occur out of thermal equilibrium. In appendix G, we show how modified production rates can be derived by considering classical plasma oscillations in the fluid approximation, including the presence of a new weakly-coupled field in addition to electromagnetism. This serves as an independent check of our thermal field theory calculations, as well as indicating how to extend them to other situations.

Future observations of stars, and of the early universe, will improve our sensitivity to anomalous energy losses, and if deviations from Standard Model predictions are found, may provide hints of new, light BSM particles. In either case, correct calculations of BSM production rates are vital in translating such observations into knowledge about new physics.

Note added. In the final stages of preparing this manuscript, the paper [25] which also studies plasma effects on supernova dark photon bounds, was posted on the arXiv.

Acknowledgments

We acknowledge helpful discussions with Asimina Arvanitaki, Masha Baryakhtar, Anthony Fradette, Junwu Huang, Maxim Pospelov, and Yu-Dai Tsai. Research at Perimeter Institute is supported by the Government of Canada through Industry Canada and by the Province of Ontario through the Ministry of Economic Development & Innovation.

A Thermal field theory — Real time formalism

In the real-time formalism of thermal field theory [10], for each physical field ϕ_1 we introduce a 'ghost' field ϕ_2, with the in-medium propagator being a matrix that mixes the $1, 2$ fields. This doubling of degrees allows the formalism to keep track of the analytic structure of the contour along which the time integral is evaluated. We can write the full in-medium propagator D_{ab} (with $a, b \in \{1, 2\}$) as

$$D_{ab}^{-1} = (D^F)_{ab}^{-1} + i\Pi_{ab}\,, \tag{A.1}$$

where D^F is the free-field propagator in the thermal bath, and Π_{ab} is the self-energy. From [10], the propagator can be diagonalised in the $\{1, 2\}$ basis by the matrix

$$U = \begin{pmatrix} \sqrt{1+n(\omega)} & \sqrt{n(\omega)} \\ \sqrt{n(\omega)} & \sqrt{1+n(\omega)} \end{pmatrix}, \tag{A.2}$$

JHEP02(2017)033

giving

$$D_{ab}(K) = U(\omega) \begin{pmatrix} \frac{i}{K^2 - m^2 - \Pi(K)} & 0 \\ 0 & \frac{-i}{K^2 - m^2 - \Pi^*(K)} \end{pmatrix} U(\omega)\,, \tag{A.3}$$

for a single species of mass M, where $\Pi(K)$ is the 'real-time' self-energy.

B Damping rates in a dilute non-relativistic plasma

For a vector coupling to electrons with coupling g, the damping rate from Thomson scattering is [7], writing $\alpha_g = g^2/4\pi$,

$$\Gamma_T \simeq \sigma_L \simeq \frac{8\pi\alpha\alpha_g n_e}{3m_e^2}\sqrt{1 - \omega_p^2/\omega^2}\,, \tag{B.1}$$

for $\omega > \omega_p$, and zero for smaller ω (since ω_p is the minimum energy carried by a SM photon in the plasma).

The damping rate from electron-ion bremsstrahlung is

$$\Gamma_T \simeq \frac{16\pi^2\alpha^2\alpha_g}{3m_e^2\omega^3}\sqrt{\frac{2\pi m_e}{3T}} n_e n_i Z_i^2 \bar{g}_i(\omega, T) \frac{1}{1 + f_B(\omega)}\,, \tag{B.2}$$

to lowest order in m_e/m_i, where $\bar{g}$ is the thermally-averaged Gaunt factor [49]. In the Born approximation,

$$\bar{g} = \frac{\sqrt{3}}{\pi} e^{\omega/(2T)} K_0(\omega/(2T))\,, \tag{B.3}$$

(this approximation is valid for $\omega \ll T$, but $\bar{g}$ is order-1 throughout). In the simplest case of emitting a massless vector, integrating over ω gives a power per unit volume of

$$\int \frac{d^3k}{(2\pi)^3} f_B(\omega)\omega\Gamma_T \simeq \sqrt{\frac{2\pi}{3}} \frac{8\alpha^2\alpha_g n_e n_i Z^2\sqrt{T}}{3m_e^{3/2}} \langle\bar{g}\rangle\ . \tag{B.4}$$

The leading-order expressions for σ_L are the same.

For a vector coupling to nucleons, we also have ion-ion bremsstrahlung. The situation here is slightly more complicated, since the ions interact through a *repulsive* Coulomb potential, rather than an attractive one as for electron-ion collisions. In the Born approximation, the damping rates are as for the attractive case, if we substitute $(X_1/m_1 - X_2/m_2)^2$ for $1/m_e^2$, and the reduced mass μ for the rest of the m_e, where m_1 and m_2 are the masses of the ions, and X_1, X_2 their charges under the new vector.

If the ion thermal velocities are low enough — in particular, if $Z_1 Z_2 e^2/v_i \gg 1$, where $v_i \sim \sqrt{T/m_i}$ is a typical ion thermal velocity — then the ion wavefunctions are significantly distorted during the collision, and the Born approximation ceases to hold. In this regime, the emission can be treated as approximately classical. [50] gives the classical dipole radiation spectrum from collisions with a given initial approach velocity v_0; for high frequencies, this is suppressed by

$$\exp\left(-\frac{\pi\alpha Z_1 Z_2}{v_0}\frac{\omega}{\mu v_0^2/2}\right)\ . \tag{B.5}$$

JHEP02(2017)033

So, in a thermal bath, emission at frequencies $\gg T\frac{v_0}{\alpha Z_1 Z_2}$ is exponentially suppressed — the Coulomb repulsion between the ions stops them from getting close enough to undergo larger accelerations. We can calculate the classical radiative energy loss analytically, obtaining

$$\frac{dP}{dV} \simeq \frac{8\pi}{3}\alpha\alpha_g Z_1 Z_2 \left(\frac{X_1 m_2 - X_2 m_1}{\sqrt{m_1 m_2}}\right)^2 \frac{T n_1 n_2}{m_1 m_2}\,, \tag{B.6}$$

for transverse radiation of a massless vector. If the plasma screening length is comparable to the ion separations during collisions, $r_0 \sim \alpha Z_1 Z_2/T$, then screening effects will become important.

C Photon self-energies in relativistic/degenerate plasmas

This appendix mostly reviews results from [11], both to collect them in a convenient form, and to allow us to extend them to mixing self-energies in appendix D.

Evaluating the real part of the one-loop electron self-energy diagram, using free field propagators for the electrons, we obtain

$$\Pi_r^{\mu\nu}(K) = e^2 \int \frac{d^3p}{(2\pi)^3}\frac{1}{2E_p}(f_e(E_p) + f_{\bar{e}}(E_p)) \times \frac{P\cdot K(P^\mu K^\mu + K^\mu P^\nu) - K^2 P^\mu P^\nu - (P\cdot K)^2 g^{\mu\nu}}{(P\cdot K)^2 - (K^2)^2/4}\,, \tag{C.1}$$

which is correct to order α. As discussed in [1, 11], the K^4 term in the denominator gives an $\mathcal{O}(\alpha^2)$ correction everywhere on the dispersion relation ('on-mass-shell'). It can therefore be ignored at leading order — this also prevents the on-mass-shell self-energy from gaining a $\mathcal{O}(\alpha^2)$ imaginary part due $\gamma \to e^+e^-$ decays, which are prevented by the electron also gaining a thermal mass [11].

Ignoring the K^4 term, we can do the angular parts of the integral, obtaining

$$\Pi_{T,r}(\omega,k) = \frac{4\alpha}{\pi}\int_0^\infty dp\, f_p \frac{p^2}{E^2}\left(\frac{\omega^2}{k^2} - \frac{\omega^2-k^2}{k^2}\frac{\omega}{2kv}\log\left(\frac{\omega+vk}{\omega-vk}\right)\right)\,, \tag{C.2}$$

$$\Pi_{L,r}(\omega,k) = \frac{4\alpha}{\pi}\frac{\omega^2-k^2}{k^2}\int_0^\infty dp\, f_p \frac{p^2}{E^2}\left(\frac{\omega}{kv}\log\left(\frac{\omega+vk}{\omega-vk}\right) - \frac{\omega^2-k^2}{\omega^2-k^2v^2} - 1\right)\,. \tag{C.3}$$

Approximating the energy integral by taking it to be dominated by a particular electron velocity v_*, we obtain the analytic approximations [11]

$$\Pi_{T,r}(\omega,k) \simeq \omega_p^2 \frac{3}{2v_*^2}\left(\frac{\omega^2}{k^2} - \frac{\omega^2 - v_*^2k^2}{k^2}\frac{\omega}{2v_*k}\log\left(\frac{\omega+v_*k}{\omega-v_*k}\right)\right)\,, \tag{C.4}$$

$$\Pi_{L,r}(\omega,k) \simeq \frac{K^2}{k^2}\omega_p^2\frac{3}{v_*^2}\left(\frac{\omega}{2v_*k}\log\left(\frac{\omega+v_*k}{\omega-v_*k}\right) - 1\right)\,, \tag{C.5}$$

where

$$\omega_p^2 \equiv \frac{4\alpha}{\pi}\int_0^\infty dp\frac{p^2}{E}f_p\left(1-\frac{1}{3}v^2\right)\,, \tag{C.6}$$

$$\omega_1^2 \equiv \frac{4\alpha}{\pi}\int_0^\infty dp\frac{p^2}{E}f_p\left(\frac{5}{3}v^2 - v^4\right)\,, \tag{C.7}$$

$$v_* \equiv \omega_1/\omega_p\,. \tag{C.8}$$

JHEP02(2017)033

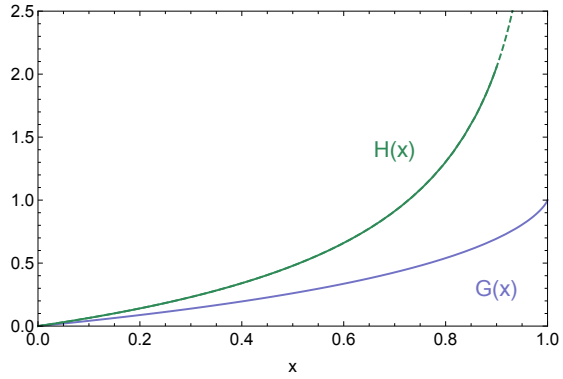

Figure 7. $G(x)$ (blue curve) and $H(x)$ (green curve), as defined in equation. (C.9) and (C.10).

These expression are accurate to order α in the degenerate ($T \ll \mu - m_e$), 'classical' ($m_e - \mu \gg T$), and relativistic ($T \gg m_e$ or $\mu \gg m_e$) limits. As per [1], if we define the functions

$$G(x) = \frac{3}{x}\left(1 - \frac{2x}{3} - \frac{1-x}{2\sqrt{x}}\log\left(\frac{1+\sqrt{x}}{1-\sqrt{x}}\right)\right) , \tag{C.9}$$

$$H(x) = \frac{G(x)-x}{x-1} = \frac{3}{2x^{3/2}}\log\left(\frac{1+\sqrt{x}}{1-\sqrt{x}}\right) - 1 - \frac{3}{x} , \tag{C.10}$$

then the above expressions are

$$\Pi_T \simeq \omega_p^2\left(1 + \frac{1}{2}G(v_*^2k^2/\omega^2)\right) , \tag{C.11}$$

$$\Pi_L \simeq \frac{K^2}{\omega^2}\omega_p^2(1 + H(v_*^2k^2/\omega^2)) . \tag{C.12}$$

We see that the dispersion relations both have $\omega = \omega_p$ at $k = 0$, and that the frequency at which the longitudinal dispersion relation crosses the lightcone goes to infinity as the electron velocity goes to one. However, the crossing frequency increases rather slowly. For example, in a SN core, with $T \simeq 30\,\mathrm{MeV}$ and $\mu_e \simeq 350\,\mathrm{MeV}$, we have $v_* \simeq 1 - 2\times10^{-6}$. On the light-cone, this gives $1 + H(v_s^2) \simeq 18.7$, and since $\omega_p \simeq 20\,\mathrm{MeV}$, the crossing frequency is $\sqrt{(1+H(v_*^2))}\omega_p \simeq 85\,\mathrm{MeV}$. In general,

$$H(1-\delta^2) \simeq 3\log\delta^{-1} + \ldots \tag{C.13}$$

To evaluate resonant longitudinal production rates (e.g. 2.21), we need the expression

$$1 - \left.\frac{d\omega_L^2}{d\omega^2}\right|_{K^2=m^2} \simeq 1 + \frac{m^2}{2k^2}\left(3 + \frac{2x^{3/2}}{(1-x)\left(2\sqrt{x} - \log\left(\frac{1+\sqrt{x}}{1-\sqrt{x}}\right)\right)}\right) , \tag{C.14}$$

where $x = v_*^2k^2/\omega^2$. For $x = 1-\delta^2$, this is

$$\simeq 1 - \frac{m^2}{2k^2\delta^2\log\delta^{-1}} + \ldots \tag{C.15}$$

Since $\delta > m^2/\omega^2$, this factor is always $\mathcal{O}(1)$.

JHEP02(2017)033

D Scalar self-energies

The one-loop electron self-energy expressions for $\phi\phi$ and ϕ-photon mixing, for a $g_\phi \phi \bar{e} e$ coupling, are

$$(\Pi^\mu)^{\phi A}(K) = g_\phi e \int \frac{d^3p}{(2\pi)^3} \frac{1}{2E_p}(f_e(E_p) + f_{\bar{e}}(E_p)) \\ m_e \frac{(P\cdot K)K^\mu - K^2 P^\mu}{(P\cdot K)^2 - (K^2)^2/4}\,, \tag{D.1}$$

$$\Pi^{\phi\phi}(K) = g_\phi^2 \int \frac{d^3p}{(2\pi)^3} \frac{1}{2E_p}(f_e(E_p) + f_{\bar{e}}(E_p)) \\ \frac{(P\cdot K)^2 - m_e^2 K^2}{(P\cdot K)^2 - (K^2)^2/4}\,, \tag{D.2}$$

(as compared to the photon-photon expression in equation (C.1)). By the same arguments as in appendix C, if we are just interested in the behaviour on the photon mass shell, or for K^2 sufficiently small, we can ignore the K^4 term in the denominator, giving

$$\Pi^{\phi L} \simeq \frac{g e m_e}{2\pi^2 k}\sqrt{K^2}\int_0^\infty dp\, v^2 f_p \left(\frac{\omega}{vk}\log\left(\frac{\omega+vk}{\omega-vk}\right) - 2\frac{K^2}{\omega^2 - k^2 v^2}\right)\,. \tag{D.3}$$

where we have written $\Pi^{\phi L} \equiv \epsilon_L^\mu (\Pi_\mu)^{\phi A}$. For a non-relativistic plasma, this gives

$$\Pi^{\phi L} \simeq g e \frac{k\sqrt{K^2}}{\omega^2}\frac{n_e}{m_e}\,, \tag{D.4}$$

in agreement with the expression in section 2.4. The $\Pi_r^{\phi L}$ self-energy is related to the resonant scalar production rate by

$$\frac{d\dot{N}}{dV} \simeq \frac{1}{4\pi}\left(\frac{\omega_L}{m}\Pi_r^{\phi L}\right)^2 \frac{1}{e^{\omega_L/T}-1}\left|1 - \frac{d\omega_L^2}{d\omega^2}\Big|_{\omega_L}\right|^{-1}\,. \tag{D.5}$$

E Decay to electrons and positrons

In appendix C, we noted that for a photon excitation of small invariant mass, the in-medium mass of the electron prevents the decay $\gamma \to e^+e^-$. However, if the new weakly coupled state has mass $m > 2\tilde{m}_e$, where $\tilde{m}_e$ is the effective electron mass, the weakly-coupled state can decay into an electron and a positron, and we need the corresponding imaginary parts of Π^{XX}, Π^{XA} and Π^{AA} to evaluate the absorption rate from this decay. The simplest case, and the only one which is relevant to the calculations in this paper, is that of a heavy dark photon, where we only need to calculate Π_i^{AA} at large invariant mass.

From [51], the effective electron mass (at $k = 0$) is

$$\tilde{m}_e = \frac{m_e}{2} + \sqrt{\frac{m_e^2}{4} + m_{\text{eff}}^2}\,, \tag{E.1}$$

JHEP02(2017)033

where

$$m_{\rm eff}^2 = \alpha \int_0^\infty EdE(f_-(E) + f_+(e) + 2f_B(E)) \tag{E.2}$$

$$= \alpha \int_0^\infty EdE \left(\frac{1}{e^{(E-\mu)/T}+1} + \frac{1}{e^{(E+\mu)/T}+1} + 2\frac{1}{e^{E/T}-1} \right) . \tag{E.3}$$

For example, in a SN core with $T = 30\,\mathrm{MeV}$, $\mu = 350\,\mathrm{MeV}$, we have $\tilde{m}_e \simeq 12\,\mathrm{MeV}$. For an ultra-relativistic electron, the dispersion relation has $\omega^2 - k^2$ ranging from $m_{\rm eff}^2$ at $k = 0$ to $2m_{\rm eff}^2$ as $k \to \infty$. The decay rate for longitudinal excitations is (ignoring the longitudinal residue factor, and in the rest frame of the plasma)

$$\Gamma_{L,\rm dec}(\omega, k) \simeq \frac{\alpha}{2\omega k} K^2 \int_{E_-}^{E^+} dE\, g(E) \left(1 - 4 \left(\frac{E}{k} - \frac{\omega}{2k} \right)^2 \right) (1 - f_-(E)) , \tag{E.4}$$

where $f_-(E) = 1/(e^{(E-\mu)/T} + 1)$ is the electron occupation number, giving Pauli blocking, $g(E)$ is an order-1 function summarising the in-medium residue factor for the electron/positron, and $E_\pm$ are the maximum and minimum decay energies in the plasma rest frame. Ignoring the frequency variation in the electron effective mass, $E_\pm = (1/2)(\omega \pm \beta_{cm} k)$, where $\beta_{cm} \equiv \sqrt{1 - 4\tilde{m}_e^2/m^2}$. For transverse excitations (again ignoring the transverse residue factor),

$$\Gamma_{T,\rm dec}(\omega, k) \simeq \frac{\alpha}{2\omega k} K^2 \int_{E_-}^{E^+} dE\, g(E) \left(1 + 2 \left(\frac{E}{k} - \frac{\omega}{2k} \right)^2 - \frac{\beta_{cm}^2}{2} \right) (1 - f_-(E)) . \tag{E.5}$$

Ignoring Pauli-blocking (i.e. setting $f_- = 0$) and residue factors, we obtain

$$\Gamma_{T,\rm dec} = \Gamma_{L,\rm dec} = \frac{\alpha}{3} \frac{m^2}{\omega} \beta \left(1 + \frac{2m_e^2}{m^2} \right) , \tag{E.6}$$

which is the correct decay rate in vacuum.

F Dark photon production and absorption in supernovae

Here we give cross sections for dark photon production and absorption in the soft approximation, following [5] but adapting to include thermal mixing effects (which requires separating the longitudinal and transverse cases).

Assuming the energy of an emitted photon is small compared to the energy of the proton-neutron interaction, the cross section for the emission of a photon can be related to that for elastic neutron-proton scattering by

$$d\sigma_{pn\to pn\gamma} \simeq -4\pi\alpha \left(\epsilon_\mu J^\mu\right)^2 \frac{d^3k}{2\omega} d\sigma_{pn\to pn}, \tag{F.1}$$

where J is the dipole current

$$J = \frac{P_1}{P_1.K} - \frac{P_2}{P_2.K} , \tag{F.2}$$

JHEP02(2017)033

with K the four-momentum of the emitted photon, and P_1 and P_2 the initial and final four-momentum of the proton. As well as a dipole contribution from neutron-proton interactions there will also be quadrupole pieces from proton-proton interactions, however these are smaller.

For the longitudinal polarisation we have

$$\frac{1}{4\pi}\int d\Omega_k\,(\epsilon\cdot J)^2 \simeq \frac{2}{3}\frac{E_{cm}}{m_n}\frac{K^2}{\omega^4}\,(1-\cos\theta_{cm})\,. \tag{F.3}$$

in the centre of mass frame, and assuming the nucleons are non-relativistic. This is suppressed by m^2/ω^2 and in the limit $m \ll \omega \sim T$ is small as expected. For the transverse modes we have, summing over the two polarisations,

$$\frac{1}{4\pi}\int d\Omega_k \sum_i (\epsilon_i\cdot J)^2 \simeq \frac{4}{3}\frac{E_{cm}}{m_n}\frac{1}{\omega^2}\,(1-\cos\theta_{cm})\,. \tag{F.4}$$

Assuming nucleons are non-degenerate in the supernova environment, the initial proton and neutron states can be integrated over. The rate of energy loss per unit volume, by continuum emission of dark photons is then given by

$$\frac{dE}{dV\,dt} = \frac{4\alpha n_n n_p}{(\pi m_n T)^{3/2}}\int_m^\infty dE\;E^3 e^{-E/T} I_{(L,T)}\,(E)\,\sigma_{np}\,(E)\;, \tag{F.5}$$

where m is the dark photon mass. The quantity

$$\sigma_{np}\,(E) = \int d\cos\theta_{cm}\;\;(1-\cos\theta_{cm})\,\frac{d\sigma_{np}}{d\cos\theta_{cm}}\,, \tag{F.6}$$

can be extracted from data and is given in [5]. The functions $I_{L,T}$ include the effects of mixing and are given by

$$I_T\,(E) = \epsilon^2\frac{m^4}{\left(m_T^2-m^2\right)^2}\frac{4}{3}\left(\sqrt{1-\left(\frac{m}{E}\right)^2}-\left(\frac{m}{E}\right)\arccos\left(\frac{m}{E}\right)\right)\,, \tag{F.7}$$

and

$$I_L\,(E) = \epsilon^2\int_m^E d\omega\;\frac{\omega^4}{\left(\omega_L^2-\omega^2\right)^2}\frac{2\sqrt{\omega^2-m^2}m^2}{3\omega^3 E}\,, \tag{F.8}$$

where the notation is the same as in section 2.1, with ω_L given by equation (C.12). As discussed in section 2.2, for resonant emission the value of the imaginary part of the photon self energy cancels out when computing the overall energy emitted.

The absorption cross sections are obtained analogously, and for the dark photon the inverse mean free path is

$$\frac{1}{\lambda_T} = \frac{32}{3\pi}\alpha n_n n_p\left(\frac{\pi T}{m_n}\right)^{3/2}\frac{1}{\omega^3\sqrt{1-\left(\frac{m}{\omega}\right)^2}}\frac{\epsilon^2 m^4}{\left(m_T^2-m^2\right)^2}\,\langle\sigma_{np}\,(T)\rangle\;, \tag{F.9}$$

for transverse modes, and

$$\frac{1}{\lambda_L} = \frac{32}{3\pi}\alpha n_n n_p\left(\frac{\pi T}{m_n}\right)^{3/2}\frac{m^2}{\omega\sqrt{1-\left(\frac{m}{\omega}\right)^2}}\frac{\epsilon^2}{\left(\omega_L^2-\omega^2\right)^2}\,\langle\sigma_{np}\,(T)\rangle\;, \tag{F.10}$$

JHEP02(2017)033

for longitudinal modes. Here

$$\langle \sigma_{np}(T) \rangle = \int_0^\infty dx \frac{1}{2} x^2 e^{-x} \sigma_{np}(xT) \ , \tag{F.11}$$

is a thermally averaged cross section, and numerical values as a function of temperature are again given in [5].[10]

G Classical equations of motion

To illustrate how our 'mixing effects' arise outside the thermal field theory formalism, we can look at the classical EoM for plasma oscillations in the fluid approximation, with the presence of an additional weakly-coupled field (as per e.g. [47]). For example, considering the case of longitudinal oscillations in the presence of a $\phi\bar{e}e$ scalar, the electric field E and scalar field ϕ are sourced by (assuming that ions have $Z = 1$)

$$\vec{\nabla} \cdot \vec{E} = -e(n_e - n_i) \quad , \quad (\partial_t^2 - \nabla^2 - m^2)\phi \simeq g n_e \, , \tag{G.1}$$

where we have assumed that the electron motions are non-relativistic. The continuity equations are

$$\dot{n}_e + \vec{\nabla} \cdot (n_e \vec{v}_e) = 0 \quad , \quad \dot{n}_i + \vec{\nabla} \cdot (n_i \vec{v}_i) = 0 \, , \tag{G.2}$$

and the momentum equations (ignoring thermal diffusion) are

$$m_e n_e (\dot{\vec{v}}_e + \vec{v}_e \cdot \vec{\nabla} \vec{v}_e) \simeq -n_e (e\vec{E} - g\vec{\nabla}\phi) - m_e n_e \nu (\vec{v}_e - \vec{v}_i) \, , \tag{G.3}$$

$$m_i n_i (\dot{\vec{v}}_i + \vec{v}_i \cdot \vec{\nabla} \vec{v}_i) \simeq n_i e\vec{E} + m_e n_e \nu (\vec{v}_i - \vec{v}_e) \, , \tag{G.4}$$

where we have included a 'frictional drag' term from electron-ion collisions, parameterised by an 'effective collision frequency' ν (we have ignored magnetic fields, since the velocities are non-relativistic).

To find the equation of motion for small oscillations, we linearise about the equilibrium values of quantities, writing $n_e = n_0(1+\delta_e)$, $n_i = n_0(1+\delta_i)$, $\phi = \phi_0 + \delta\phi$, and and v_e, v_i, E as small quantities themselves. Taking the limit where the ion mass is much heavier than the electron mass, we can set $v_i, \delta_i = 0$ throughout. Writing the linearised quantities as $e^{-i(\omega t - kx)}$ (i.e. taking propagation to be in the x direction), and solving for v_e, δ_e in terms of $E, \delta\phi$, we obtain the equations

$$\left(\begin{pmatrix} -ik & 0 \\ 0 & \omega^2 - k^2 - m^2 \end{pmatrix} - \frac{n_0}{m_e} \frac{k}{\omega(\omega - i\nu)} \begin{pmatrix} -ie^2 & egk \\ ieg & -g^2 k \end{pmatrix} \right) \begin{pmatrix} E \\ \delta\phi \end{pmatrix} = 0 \ . \tag{G.5}$$

For $g = 0$, we obtain the separate equations

$$1 - \frac{\omega_p^2}{\omega(\omega - i\nu)} \quad \Rightarrow \quad \omega = \sqrt{\omega_p^2 - \frac{\nu^2}{4\omega_p^2}} + \frac{i\nu}{2} \, , \tag{G.6}$$

[10] Our expressions match those of [25] and differ from those of [5] by numerical factors.

JHEP02(2017)033

for E, and $\omega^2 - k^2 - m^2 = 0$ for $\delta\phi$, as expected. With $g \neq 0$, if we write $\omega = \sqrt{k^2 + m^2} + g^2\omega_g \equiv \omega_0 + g^2\omega_g$, then the weakly-coupled mode has

$$\mathrm{Im}\,\omega_g = -k^2 \frac{n_0}{2m_e} \frac{\nu}{\omega_0^2\nu^2 + (\omega_0^2 - \omega_p^2)^2} \,. \tag{G.7}$$

Around the resonance, when $\omega_0 \simeq \omega_p$, this has the form of equation (2.30), since as per above, $\sigma_L \simeq \nu$ there. This confirms that the resonant production is not m-suppressed for small m. Inserting the general relationship between ν and σ_L into equation (G.7), we obtain equation (2.30), as required.

Analogous calculations can be done for the new particle candidates discussed in this work, replicating the results of the thermal field theory calculations as required.

References

[1] G.G. Raffelt, *Stars as laboratories for fundamental physics*, Chicago University Press, Chicago U.S.A. (1996).

[2] E.D. Carlson, *Limits on a new* U(1) *coupling*, *Nucl. Phys.* **B 286** (1987) 378 [INSPIRE].

[3] J.A. Grifols, E. Masso and S. Peris, *Energy loss from the sun and RED giants: bounds on short range baryonic and leptonic forces*, *Mod. Phys. Lett.* **A 4** (1989) 311 [INSPIRE].

[4] J.B. Dent, F. Ferrer and L.M. Krauss, *Constraints on light hidden sector gauge bosons from supernova cooling*, arXiv:1201.2683 [INSPIRE].

[5] E. Rrapaj and S. Reddy, *Nucleon-nucleon bremsstrahlung of dark gauge bosons and revised supernova constraints*, *Phys. Rev.* **C 94** (2016) 045805 [arXiv:1511.09136] [INSPIRE].

[6] H. An, M. Pospelov and J. Pradler, *New stellar constraints on dark photons*, *Phys. Lett.* **B 725** (2013) 190 [arXiv:1302.3884] [INSPIRE].

[7] J. Redondo and G. Raffelt, *Solar constraints on hidden photons re-visited*, *JCAP* **08** (2013) 034 [arXiv:1305.2920] [INSPIRE].

[8] J. Redondo and M. Postma, *Massive hidden photons as lukewarm dark matter*, *JCAP* **02** (2009) 005 [arXiv:0811.0326] [INSPIRE].

[9] D. Kazanas, R.N. Mohapatra, S. Nussinov, V.L. Teplitz and Y. Zhang, *Supernova bounds on the dark photon using its electromagnetic decay*, *Nucl. Phys.* **B 890** (2014) 17 [arXiv:1410.0221] [INSPIRE].

[10] M.L. Bellac, *Thermal field theory*, Cambridge University Press, Cambridge U.K. (2011).

[11] E. Braaten and D. Segel, *Neutrino energy loss from the plasma process at all temperatures and densities*, *Phys. Rev.* **D 48** (1993) 1478 [hep-ph/9302213] [INSPIRE].

[12] J. Redondo, *Helioscope bounds on hidden sector photons*, *JCAP* **07** (2008) 008 [arXiv:0801.1527] [INSPIRE].

[13] F.F. Chen, *Introduction to plasma physics and controlled fusion*, Springer, Germany (1984).

JHEP02(2017)033

[14] S. Alekhin et al., *A facility to search for hidden particles at the CERN SPS: the SHiP physics case*, *Rept. Prog. Phys.* **79** (2016) 124201 [arXiv:1504.04855] [INSPIRE].

[15] P. Gondolo and G. Raffelt, *Solar neutrino limit on axions and keV-mass bosons*, *Phys. Rev.* **D 79** (2009) 107301 [arXiv:0807.2926] [INSPIRE].

[16] N. Vinyoles et al., *New axion and hidden photon constraints from a solar data global fit*, *JCAP* **10** (2015) 015 [arXiv:1501.01639] [INSPIRE].

[17] N. Viaux et al., *Neutrino and axion bounds from the globular cluster M5 (NGC 5904)*, *Phys. Rev. Lett.* **111** (2013) 231301 [arXiv:1311.1669] [INSPIRE].

[18] A. Ayala, I. Domínguez, M. Giannotti, A. Mirizzi and O. Straniero, *Revisiting the bound on axion-photon coupling from Globular Clusters*, *Phys. Rev. Lett.* **113** (2014) 191302 [arXiv:1406.6053] [INSPIRE].

[19] B. Müller, *The status of multi-dimensional core-collapse supernova models*, arXiv:1608.03274 [INSPIRE].

[20] K. Blum and D. Kushnir, *Neutrino signal of collapse-induced thermonuclear supernovae: the case for prompt black hole formation in SN1987A*, *Astrophys. J.* **828** (2016) 31 [arXiv:1601.03422] [INSPIRE].

[21] W. Keil, H.T. Janka and G. Raffelt, *Reduced neutrino opacities and the SN1987A signal*, *Phys. Rev.* **D 51** (1995) 6635 [hep-ph/9410229] [INSPIRE].

[22] H.-T. Janka, *Explosion mechanisms of core-collapse supernovae*, *Ann. Rev. Nucl. Part. Sci.* **62** (2012) 407 [arXiv:1206.2503] [INSPIRE].

[23] C. Hanhart, J.A. Pons, D.R. Phillips and S. Reddy, *The likelihood of GODs' existence: improving the SN1987a constraint on the size of large compact dimensions*, *Phys. Lett.* **B 509** (2001) 1 [astro-ph/0102063] [INSPIRE].

[24] A. Kopf and G. Raffelt, *Photon dispersion in a supernova core*, *Phys. Rev.* **D 57** (1998) 3235 [astro-ph/9711196] [INSPIRE].

[25] J.H. Chang, R. Essig and S.D. McDermott, *Revisiting supernova 1987A constraints on dark photons*, *JHEP* **01** (2017) 107 [arXiv:1611.03864] [INSPIRE].

[26] A. Fradette, M. Pospelov, J. Pradler and A. Ritz, *Cosmological constraints on very dark photons*, *Phys. Rev.* **D 90** (2014) 035022 [arXiv:1407.0993] [INSPIRE].

[27] J. Berger, K. Jedamzik and D.G.E. Walker, *Cosmological constraints on decoupled dark photons and dark Higgs*, *JCAP* **11** (2016) 032 [arXiv:1605.07195] [INSPIRE].

[28] R. Essig et al., *Working group report: new light weakly coupled particles*, in the proceedings of the *Community Summer Study 2013: Snowmass on the Mississippi (CSS2013)*, July 29–August 6, Minneapolis, U.S.A. (2013), arXiv:1311.0029 [INSPIRE].

[29] NA64 collaboration, D. Banerjee et al., *Search for invisible decays of sub-GeV dark photons in missing-energy events at the CERN SPS*, *Phys. Rev. Lett.* **118** (2017) 011802 [arXiv:1610.02988] [INSPIRE].

[30] A.D. Dolgov, S.H. Hansen, G. Raffelt and D.V. Semikoz, *Cosmological and astrophysical bounds on a heavy sterile neutrino and the KARMEN anomaly*, *Nucl. Phys.* **B 580** (2000) 331 [hep-ph/0002223] [INSPIRE].

[31] A. Burrows, M.T. Ressell and M.S. Turner, *Axions and SN1987A: axion trapping*, *Phys. Rev.* **D 42** (1990) 3297 [INSPIRE].

JHEP02(2017)033

[32] R.S. Decca, D. Lopez, E. Fischbach, G.L. Klimchitskaya, D.E. Krause and V.M. Mostepanenko, *Novel constraints on light elementary particles and extra-dimensional physics from the Casimir effect*, *Eur. Phys. J.* **C 51** (2007) 963 [arXiv:0706.3283] [INSPIRE].

[33] A.O. Sushkov, W.J. Kim, D.A.R. Dalvit and S.K. Lamoreaux, *New experimental limits on non-newtonian forces in the micrometer range*, *Phys. Rev. Lett.* **107** (2011) 171101 [arXiv:1108.2547] [INSPIRE].

[34] A.A. Geraci, S.J. Smullin, D.M. Weld, J. Chiaverini and A. Kapitulnik, *Improved constraints on non-Newtonian forces at 10 microns*, *Phys. Rev.* **D 78** (2008) 022002 [arXiv:0802.2350] [INSPIRE].

[35] D.J. Kapner et al., *Tests of the gravitational inverse-square law below the dark-energy length scale*, *Phys. Rev. Lett.* **98** (2007) 021101 [hep-ph/0611184] [INSPIRE].

[36] J.K. Hoskins, R.D. Newman, R. Spero and J. Schultz, *Experimental tests of the gravitational inverse square law for mass separations from* 2*-cm to* 105*-cm*, *Phys. Rev.* **D 32** (1985) 3084 [INSPIRE].

[37] R. Harnik, J. Kopp and P.A.N. Machado, *Exploring ν signals in dark matter detectors*, *JCAP* **07** (2012) 026 [arXiv:1202.6073] [INSPIRE].

[38] J. Heeck, *Unbroken B-L symmetry*, *Phys. Lett.* **B 739** (2014) 256 [arXiv:1408.6845] [INSPIRE].

[39] H. An, M. Pospelov and J. Pradler, *Dark matter detectors as dark photon helioscopes*, *Phys. Rev. Lett.* **111** (2013) 041302 [arXiv:1304.3461] [INSPIRE].

[40] H. An, M. Pospelov, J. Pradler and A. Ritz, *Direct detection constraints on dark photon dark matter*, *Phys. Lett.* **B 747** (2015) 331 [arXiv:1412.8378] [INSPIRE].

[41] D. Dearborn, G. Raffelt, P. Salati, J. Silk and A. Bouquet, *Dark matter and thermal pulses in horizontal branch stars*, *Astrophys. J.* **354** (1990) 568 [INSPIRE].

[42] B. Paxton, L. Bildsten, A. Dotter, F. HERWIG, P. Lesaffre and F. Timmes, *Modules for Experiments in Stellar Astrophysics (MESA)*, *Astrophys. J. Suppl.* **192** (2011) 3 [arXiv:1009.1622] [INSPIRE].

[43] S. Dawson and H.E. Haber, *A primer on Higgs boson low-energy theorems*, talk given at the *Workshop on High-energy Physics Phenomenology (WHEPP)*, January 2–5, Bombay, India (1989).

[44] T. Flacke, C. Frugiuele, E. Fuchs, R.S. Gupta and G. Perez, *Phenomenology of relaxion-Higgs mixing*, arXiv:1610.02025 [INSPIRE].

[45] P.W. Graham, D.E. Kaplan, J. Mardon, S. Rajendran and W.A. Terrano, *Dark matter direct detection with accelerometers*, *Phys. Rev.* **D 93** (2016) 075029 [arXiv:1512.06165] [INSPIRE].

[46] J.C. Wheeler and S. Akiyama, *Magnetic fields in core collapse supernovae: Possibilities and gaps*, astro-ph/0412382 [INSPIRE].

[47] S. Dubovsky and G. Hernández-Chifflet, *Heating up the galaxy with hidden photons*, *JCAP* **12** (2015) 054 [arXiv:1509.00039] [INSPIRE].

[48] S. Chaudhuri, P.W. Graham, K. Irwin, J. Mardon, S. Rajendran and Y. Zhao, *Radio for hidden-photon dark matter detection*, *Phys. Rev.* **D 92** (2015) 075012 [arXiv:1411.7382] [INSPIRE].

JHEP02(2017)033

[49] P.J. Brussaard and H.C. van de Hulst, *Approximation formulas for nonrelativistic Bremsstrahlung and average gaunt factors for a Maxwellian electron gas*, *Rev. Mod. Phys.* **34** (1962) 507 [INSPIRE].

[50] L.D. Landau and E.M. Lifshitz, *The classical theory of fields*, 2nd edition, Course of theoretical physics. Pergamon, London U.K. (1962).

[51] E. Braaten, *Neutrino emissivity of an ultrarelativistic plasma from positron and plasmino annihilation*, *Astrophys. J.* **392** (1992) 70.

JHEP02(2017)033